iScience

CellPress
OPEN ACCESS

Article

High-throughput rational design of the remdesivir binding site in the RdRp of SARS-CoV-2: implications for potential resistance

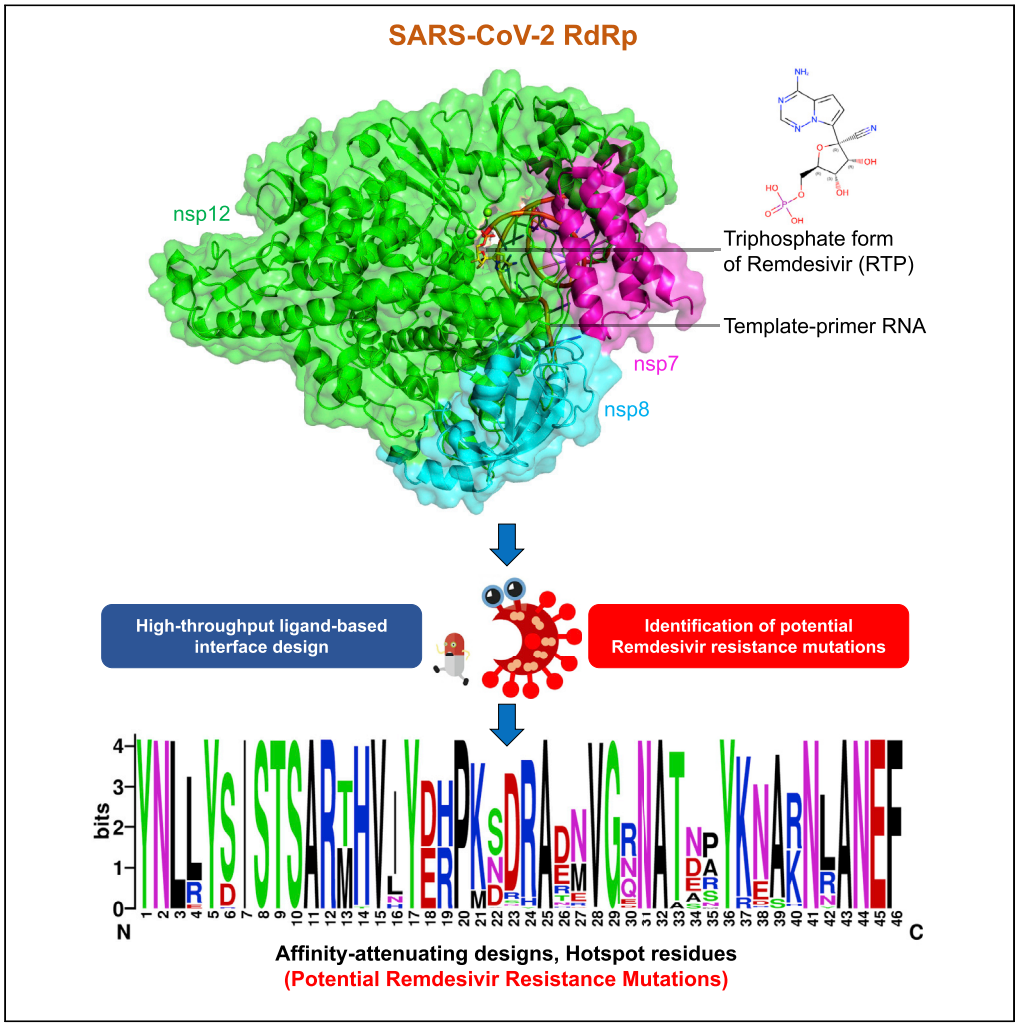

Aditya K. Padhi,
Rohit Shukla,
Prakash Saudagar,
Timir Tripathi

ps@nitw.ac.in (P.S.)
timir.tripathi@gmail.com (T.T.)

HIGHLIGHTS

SARS-CoV-2 may acquire mutations in nsp12 to develop remdesivir resistance

Hotspot residues that exhibited the highest potential for mutation were identified

Virus can undergo positive selection and attain resistance with very few mutations

Data is crucial for the understanding and management of drug resistance

Padhi et al., iScience *24*, 101992
January 22, 2021 © 2020
https://doi.org/10.1016/j.isci.2020.101992

iScience

CellPress
OPEN ACCESS

Article

High-throughput rational design of the remdesivir binding site in the RdRp of SARS-CoV-2: implications for potential resistance

Aditya K. Padhi,[1] Rohit Shukla,[2] Prakash Saudagar,[3,*] and Timir Tripathi[4,5,*]

SUMMARY

The use of remdesivir to treat COVID-19 will likely continue before clinical trials are completed. Due to the lengthening pandemic and evolving nature of the virus, predicting potential residues prone to mutation is crucial for the management of remdesivir resistance. Using a rational ligand-based interface design complemented with mutational mapping, we generated a total of 100,000 mutations and provided insight into the functional outcomes of mutations in the remdesivir-binding site in nsp12 subunit of RdRp. After designing 46 residues in the remdesivir-binding site of nsp12, the designs retained 97%–98% sequence identity, suggesting that very few mutations in nsp12 are required for SARS-CoV-2 to attain remdesivir resistance. Several mutants displayed decreased binding affinity to remdesivir, suggesting drug resistance. These hotspot residues had a higher probability of undergoing selective mutation and thus conferring remdesivir resistance. Identifying the potential residues prone to mutation improves our understanding of SARS-CoV-2 drug resistance and COVID-19 pathogenesis.

INTRODUCTION

The novel coronavirus disease (COVID-19) is a highly infectious acute respiratory disease that is caused by severe acute respiratory syndrome coronavirus-2 (SARS-CoV-2). SARS-CoV-2 is closely related to other coronaviruses (CoVs), such as SARS-CoV and bat and pangolin CoVs. However, evolutionary genomics indicates that the affinity of the Spike protein (S-protein) of SARS-CoV-2 for its human receptor angiotensin-converting enzyme 2 (ACE2) is much higher than that in other CoVs, which results in a higher infectivity rate of SARS-CoV-2 (Andersen et al., 2020; Guo et al., 2020). The genome of SARS-CoV-2 encodes four structural proteins [spike glycoprotein (S), an envelope protein (E), membrane glycoprotein (M), and nucleocapsid phosphoprotein (N)] and six nonstructural proteins [open reading frame 1ab (ORF1a and ORF1ab), ORF3a, ORF6, ORF7a, ORF8, and ORF10] (Lu et al., 2020). The cleavage of ORF1a and ORF1ab polyproteins produces various nonstructural proteins (nsps) that are involved in viral transcription and replication (Ziebuhr, 2005). Nsp12 is the catalytic subunit and core component of the RNA-dependent RNA polymerase (RdRp) of CoVs. Nsp12 forms a complex with two additional proteins, nsp7 and nsp8, and participates in the RNA template-dependent synthesis of viral RNA in the presence of divalent metal ions (Figure 1A) (Ahn et al., 2012; Subissi et al., 2014; te Velthuis et al., 2010). The binding of nsp12 to nsp7 and nsp8 enhances the template binding and processivity of nsp12 (Kirchdoerfer and Ward, 2019; Subissi et al., 2014). The structure of SARS-CoV-2 nsp12 shares high level of homology with the nsp12 of SARS-CoV (sequence identity: 96.4%; sequence similarity: 99.4%), which indicates that they have similar functions and mechanisms of action (Wu et al., 2020).

The structures of the RdRp (nsp12-nsp7-nsp8) in the apo-form (Gao et al., 2020; Kirchdoerfer and Ward, 2019) and in complex with the template primer RNA, remdesivir, and Mg^{2+} ions have been determined (Figure 1A) (Yin et al., 2020). The N-terminus of the nsp12 polymerase has a β-hairpin structure (residues 31–50) and an extended nidovirus RdRp-associated nucleotidyltransferase domain (NiRAN, residues 115–250) that consists of seven α-helices and three β-strands (Figure 1A) (Gao et al., 2020; Kirchdoerfer and Ward, 2019; Lehmann et al., 2015). The NiRAN domain binds at the backside of the cupped right-handed C-terminal RdRp via an interface domain (residues 251–365) that links the NiRAN domain to the finger subdomain of the C-terminal RdRp. The C-terminal RdRp (residues 366–920) is divided into three subdomains—finger (residues 398–581 and 621–679), palm (residues 582–627 and 688–815), and thumb (residues

[1]Laboratory for Structural Bioinformatics, Center for Biosystems Dynamics Research, RIKEN, Yokohama, Kanagawa 230-0045, Japan

[2]Department of Biotechnology and Bioinformatics, Jaypee University of Information Technology, Waknaghat, Solan 173234, India

[3]Department of Biotechnology, National Institute of Technology, Warangal 506004, India

[4]Molecular and Structural Biophysics Laboratory, Department of Biochemistry, North-Eastern Hill University, Shillong 793022, India

[5]Lead contact

*Correspondence: ps@nitw.ac.in (P.S.), timir.tripathi@gmail.com (T.T.)

https://doi.org/10.1016/j.isci.2020.101992

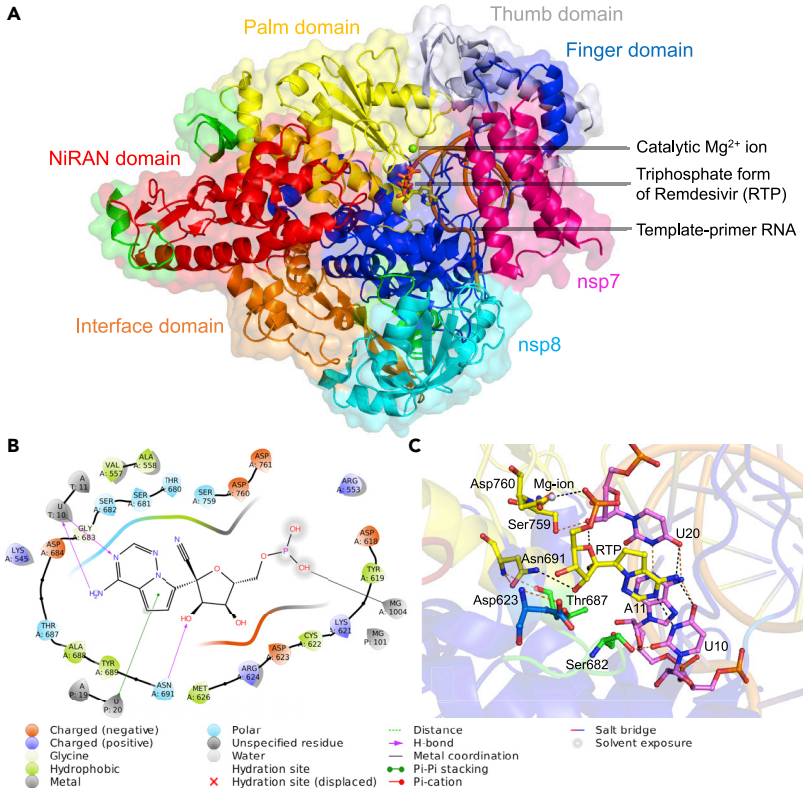

Figure 1. Structure of the nsp12-nsp7-nsp8 complex bound to the template-primer RNA and triphosphate form of remdesivir (RTP) and the RTP-interacting residues

(A) The cryo-electron microscopy structure of the RNA-dependent RNA polymerase from SARS-CoV-2 (PDB ID: 7BV2) consisting of nsp12-nsp7-nsp8 complex bound to template-primer RNA, the triphosphate form of remdesivir (RTP), and the catalytic Mg^{2+} ion is shown. Here nsp7 and nps8 are shown in magenta and cyan colors, respectively. The nsp12 subunit is comprised of several subdomains, where the NiRAN domain from residues 115-250 is shown in red color and the interface domain from residues 251–365 is shown in orange color. The C-terminal comprising residues 366–920 is divided into three subdomains, where finger domain (residues 398–581 and 621–679), palm domain (residues 582–627 and 688–815), and thumb domain (residues 816–919) are shown in blue, yellow, and blue-white colors, respectively. The triphosphate form of remdesivir (RTP) is shown as a stick model.

(B) Ligand interaction diagram of remdesivir within a 6-Å distance of the nsp12-nsp7-nsp8 complex bound to the template-primer RNA is shown, and the types of intermolecular interactions are labeled.

(C) Interacting residues of corresponding nsp12 subdomains (green, blue, and yellow) and RNA bases (violet) of remdesivir (yellow) are labeled and shown as stick models. The Mg^{2+} (gray sphere) coordinating the RTP is shown. Hydrogen bond and salt bridge interactions are shown as black and orange dashes, respectively.

816–919)—which is a conserved architecture in all viral RdRps. The long finger extension of CoV RdRp intersects with the thumb subdomain to form a closed ring structure. This conformation is in contrast to the smaller loop in the RdRp of other RNA viruses, such as influenza virus, that have a relatively open conformation. Two zinc ions also bind in the conserved metal-binding motif in all CoV RdRps and play a crucial role in maintaining RdRp stability and structural integrity (Kirchdoerfer and Ward, 2019). The overall structural architecture of the apo-RdRp (without remdesivir) and complex-RdRp (with remdesivir) is similar, except that nsp12 is in the closed conformation in apo-RdRp. The binding of nsp7 and nsp8 stabilizes the closed conformation. Remdesivir, in its monophosphate form (RMP), forms a covalent bond with the 3′ end of the RNA primer strand at the +1 position (via base-stacking interactions) and with the uridine base from the template strand (via two hydrogen bonds). RMP also interacts with side chains from Lys545 and Arg555. Two Mg^{2+} ions and one pyrophosphate are present near the bound RMP (Figure 1B). The Mg^{2+} ions interact with the phosphodiester backbone and form part of the active site (Figure 1B). The residues constituting the catalytic site and the residues involved in RNA binding are highly conserved in CoVs. Most RdRp inhibitors interact with the residues of these conserved motifs. Remdesivir is an antiviral nucleotide analog prodrug. Upon diffusion into a cell, it is converted to GS-441524 monophosphate, which

is phosphorylated to the active nucleotide triphosphate form of remdesivir (RTP). Binding of RTP leads to the inhibition of RdRp activity via nonobligate RNA chain termination (Gordon et al., 2020; Tchesnokov et al., 2019). RTP covalently binds to the +1 position and delays chain termination between positions +3 and +5. RTP inhibits the RdRp of SARS-CoV and SARS-CoV-2 with similar efficiencies and mechanisms of action (Gordon et al., 2020). Another study utilizing a cell-based assay showed that a nucleoside analog inhibitor Molnupiravir (EIDD-2801) was effective against remdesivir-resistant SARS-CoV-2. Molnupiravir reduced the replication and pathogenesis of CoVs in a manner similar to remdesivir (Sheahan et al., 2020). A recent study showed that Molnupiravir can block virus transmission in ferrets within 24 h of oral administration (Cox et al., 2020).

RNA viruses exploit all known mechanisms of genetic variation to ensure their survival. They have a remarkable ability to adapt to new hosts, environments, and drugs via the development of genetic variations in a short period of time (Domingo and Holland, 1997; Duffy, 2018). Recent data have revealed that several residues in nsp12 are mutated in SARS-CoV-2 (http://cov-glue.cvr.gla.ac.uk/#/replacement), indicating that the virus has high potential to mutate (Callaway, 2020; Padhi and Tripathi, 2020). Mutations in the remdesivir-binding site in nsp12 may induce resistance against the drug. In contrast to the investigation of mutations after drug exposure, it is useful to predict resistance mutations to guide the drug discovery and development processes and to overcome the effects of possible resistance mutations. In recent years, several sophisticated algorithms to computationally engineer proteins have been developed and used for protein design to predict potential resistance mutations (Cao et al., 2005; Frey et al., 2010; Reeve et al., 2015). Here, we used Rosetta-based high-throughput computational approaches (Alford et al., 2017; Fleishman et al., 2011; Kaufmann and Meiler, 2012; Moretti et al., 2016) to design remdesivir-binding sites in nsp12 and identify affinity-attenuating mutations. The data provide crucial insights into the residues that showed a very high tendency to undergo positive selection leading to remdesivir resistance. This work is important to understand and manage remdesivir resistance and may guide scientists in rational structure-based drug discovery.

RESULTS

Interacting residues between nsp12 and remdesivir

The interacting residues between nsp12 and remdesivir were obtained from the cryo-EM structure of the SARS-CoV-2 RdRp. A total of 56 residues from nsp12 interacted with remdesivir (Figure 1A). Notably, certain nsp12 residues, such as Ala558, Gly559, Ser682, Gly683, Asp684, Ser759, Asp760, Asp761, Cys813, and Ser814, interacted with remdesivir and template-primer RNA and were essential for maintaining the catalytic activity of RdRp. A ligand-interaction diagram further revealed that the crucial residues of nsp12 were located within a 6-Å distance of remdesivir; this highlighted the metal coordination with Mg^{2+}, hydrogen bonds with Asn691 and U10 of RNA, and a pi-pi stacking interaction with U20 of the template-primer RNA (Figures 1B and 1C).

Ligand-based interface design of the remdesivir-bound nsp12-nsp7-nsp8-RNA complex and associated physicochemical features of the complex

We performed a ligand-based interface design of the remdesivir-binding site residues of the nsp12-nsp7-nsp8-RNA complex. Remdesivir formed key contacts and interactions with 56 residues of nsp12. Notably, 10 of these 56 residues also interacted with template-primer RNA and were involved in catalytic activity. Therefore, the remaining 46 interface residues of remdesivir that bound nsp12 were designed to allow for backbone flexibility of nsp12, and the residues of nsp12 other than the interface residues were repacked. A total of 50,000 designs from the interface design were computed and analyzed for Rosetta's total scores, root-mean-square deviation (RMSD), interface delta, and percentage sequence identity. The Rosetta total score is the weighted sum of various energy terms, including physical forces such as electrostatics and van der Waals' interactions, and several other statistical terms. Rosetta interface delta represents the binding affinity between the designed nsp12 with remdesivir. The percentage sequence identity denotes the identity of the designed sequences to that of the native sequence.

First, the 50,000 designs of remdesivir-bound nsp12 were sampled by computing the total scores versus the RMSD, and all of the designs exhibited RMSD <1.5 Å (Figure 2A). Notably, more than half of the top-scoring designs showed deviations in their RMSDs below 0.5 Å, which suggests that the designs did not deviate significantly from the starting complex structure during repacking, backbone movements, and packing and maintained their structural integrity even after the introduction of mutations in the 46 interface residues

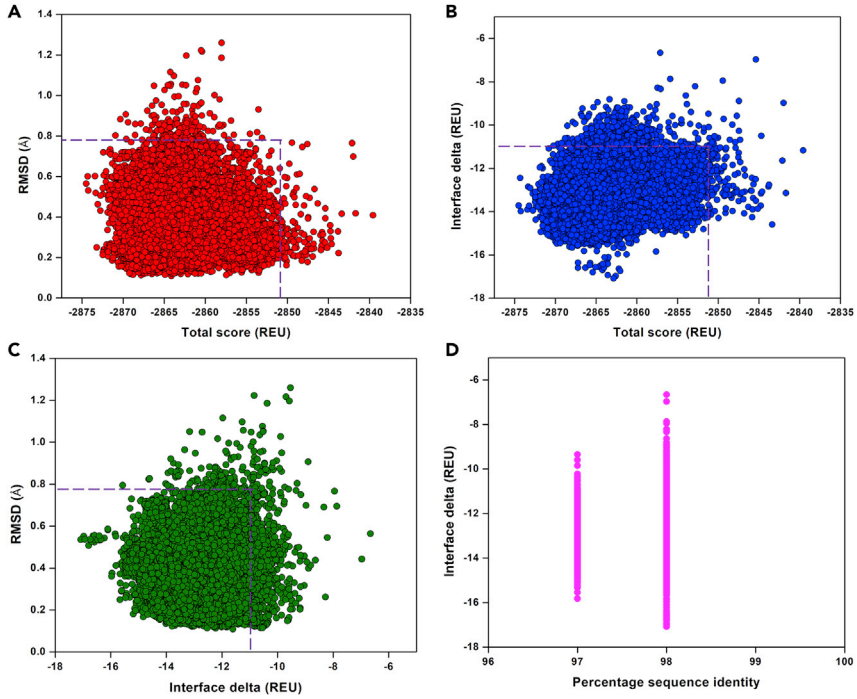

Figure 2. Structural and physicochemical parameters from the ligand-based Rosetta interface design experiment

(A) Rosetta total score versus RMSD of the 50,000 designs of remdesivir-bound nsp12-nsp7-nsp8 complex bound to the template-primer RNA complex obtained from ligand-based interface design.

(B) Rosetta total score versus interface delta representing the binding affinities of the designs between remdesivir and the nsp12-nsp7-nsp8-RNA complex.

(C) Interface delta versus RMSD of the designs, where only the remdesivir-interacting 46 residues were designed and remaining residues were repacked.

(D) Interface delta versus percentage sequence identity of the remdesivir-interacting residues of nsp12-nsp7-nsp8-RNA complex showing the distribution of designs. In panels (A–C), the dotted boxes denote the control values in which the remdesivir-interacting residues were only repacked and not designed.

of nsp12 (Figure 2A). To filter the affinity-attenuating designs from the affinity-enhancing designs, we performed a control experiment in which we only repacked (without designing) the same 46 residues of nsp12. We noted that there were designs that had poorer total scores than the control and relatively higher RMSDs even compared with the affinity-enhancing designs, which suggests that the affinity-attenuating designs exhibited slight deviation in their overall structure from the starting structure and reached unfavorable energetic states upon mutation.

Second, the binding affinity of the designs, represented as the interface delta, was computed and plotted against the total scores (Figure 2B). The affinity-attenuating designs had a significantly lower binding affinity than the affinity-enhancing designs and the control in the design calculations (Figure 2B).

Third, our computation of the RMSD versus the interface delta of the 50,000 designs revealed that the designs with lower binding affinities exhibited relatively higher RMSDs (Figure 2C). Although a considerable number of the designed structures had improved binding affinities, several designed structures had reduced binding affinities with RMSDs above 0.8 Å compared with the control group structures without design, suggesting that the mutations destabilized the intermolecular interactions with remdesivir (Figure 2C).

Finally, we evaluated the interface delta of the designs to compare the binding affinities with the sequence identities from the native sequence. Although remdesivir had contacts with many nsp12 residues, only a few of the nsp12 residues were more prone to mutations (Figure 2D). The designs exhibited an overall sequence identity of 97% and 98%, indicating several of the lower-affinity binders with 1 and 2 mutations. This result suggests that although nsp12 may acquire fewer mutations at the remdesivir-binding

site, certain residues are highly prone to mutations and develop resistance against remdesivir. However, these residues can mutate whenever the virus experiences evolutionary and immune pressure during evolution.

Validation of ligand-based interface design protocol

To validate the predictive quality and accuracy of our ligand-based interface design methodology, a previously reported remdesivir-resistant mutant of SARS-CoV, V557L, was examined (Sheahan et al., 2020). Val557 of nsp12 is conserved in SARS-CoV-2, and it may mutate to Leu557 or any other remdesivir-resistant mutation. To examine whether our methodology would recognize and rank order Leu557 as one of the low-affinity designs, we scored and scanned residues in the 557th position and found that V557L was ranked as a low-affinity design in the design calculations (Figure S1). This result demonstrated that our methodology was capable of scoring, rank-ordering, and filtering the resistance-enhancing mutations from that of the possible resistance-attenuating mutations. However, as V557L is a remdesivir-resistant mutation of SARS-CoV and not of SARS-CoV-2, it is possible that SARS-CoV-2 may not mutate the Val557 to acquire resistance; rather, any of the other 10 hotspot residues may be mutated to possibly confer resistance.

Sequence diversity of remdesivir-nsp12 binding designs

The 50,000 designs that were generated surrounding the remdesivir-binding site of nsp12 were classified as either affinity-attenuating or affinity-enhancing designs. The 46 interacting amino acid residues of the 100 top-scoring affinity-attenuating designs were analyzed and compared with the 100 top-scoring affinity-enhancing designs with a higher total score and binding affinities. A mutational landscape analysis revealed that residues Tyr456, Asn543-Ser549, Lys551, Ala553-Thr556, Val560, Trp617-Cys622, Ala625, Val662, Gly679, Ser681, Ala685, Thr686, Tyr689, Ala690, Phe694, Asn695, Ala762, Asn790, Glu811, and Phe812 were sampled to almost identical residues in both groups, and they varied most at the remaining residues (Figure 3). Notably, although some residues, such as Asp623, Asn691, and Ser692, exhibited diverse mutations between the two groups but with a smaller number of amino acids sampled in these positions, other residues, including Val557, Ile589, Met626, Arg631, Thr680, Thr687, Ala688, and Leu758, experienced more diverse sequence variations between the two groups with a relatively higher number of amino acids sampled (Figure 3). Notably, certain sites of the finger and palm residues were more prone and highly susceptible to mutations, and the catalytic and primer RNA interacting residues were completely conserved (Figure 3). Eleven residue positions of nsp12 varied between the affinity-attenuating and affinity-enhancing designs. This mutational landscape data between the affinity-attenuating and affinity-enhancing designs showed that certain amino acids and positions in the nsp12 were highly prone to mutations and even accommodated a higher number of variations. For example, the Ile589, Thr680, Thr687, Ala688, Asn691, and Leu758 sites that were sampled in the affinity-attenuating designs were already found to be mutated in the SARS-CoV-2 genomes, as reported in the CoV-GLUE database (Figure 3), which contains replacements, insertions, and deletions, and were observed in the GISAID hCoV-19 sequences sampled from patients infected with the virus (http://cov-glue.cvr.gla.ac.uk/#/replacement) (Hadfield et al., 2018). There is a high probability that once the virus comes under evolutionary and remdesivir-induced pressure, these hotspot residues will undergo the missense mutations that are observed in the affinity-attenuating designs (Figure 3). This sequence-specific conservation and diversity of the remdesivir-bound nsp12 designs show the design accuracy and predictive capability of our design methodology, which suggests that these hotspot residues will likely undergo selective mutation in the near future to develop resistance to remdesivir and related drugs, facilitating the propagation of infection and survival of SARS-CoV-2.

Binding affinity of remdesivir-bound nsp12 designs using PRODIGY-LIG

After the Rosetta ligand-based interface design calculations, we computed the binding affinities between remdesivir and all of the Rosetta-generated designs using PRODIGY-LIG. We found that the binding affinities of remdesivir-bound designs ranged from −5.01 kcal/mol to −6.35 kcal/mol (Figure S2). Several affinity-attenuating designs generated from Rosetta also had lower binding affinities in PRODIGY-LIG scoring, thus indicating good correlation and prediction accuracy across different methods. For the wild-type remdesivir-bound nsp12-nsp7-nsp8-RNA complex, the binding affinity between nsp12 and remdesivir was −6.02 kcal/mol, with a total of 2,862 atomic contacts. Interestingly, although many of the top designs had a substantial increase in binding affinity, there were several affinity-attenuating designs with reduced binding affinity with remdesivir (Figure S2).

Top 100 affinity enhancing designs

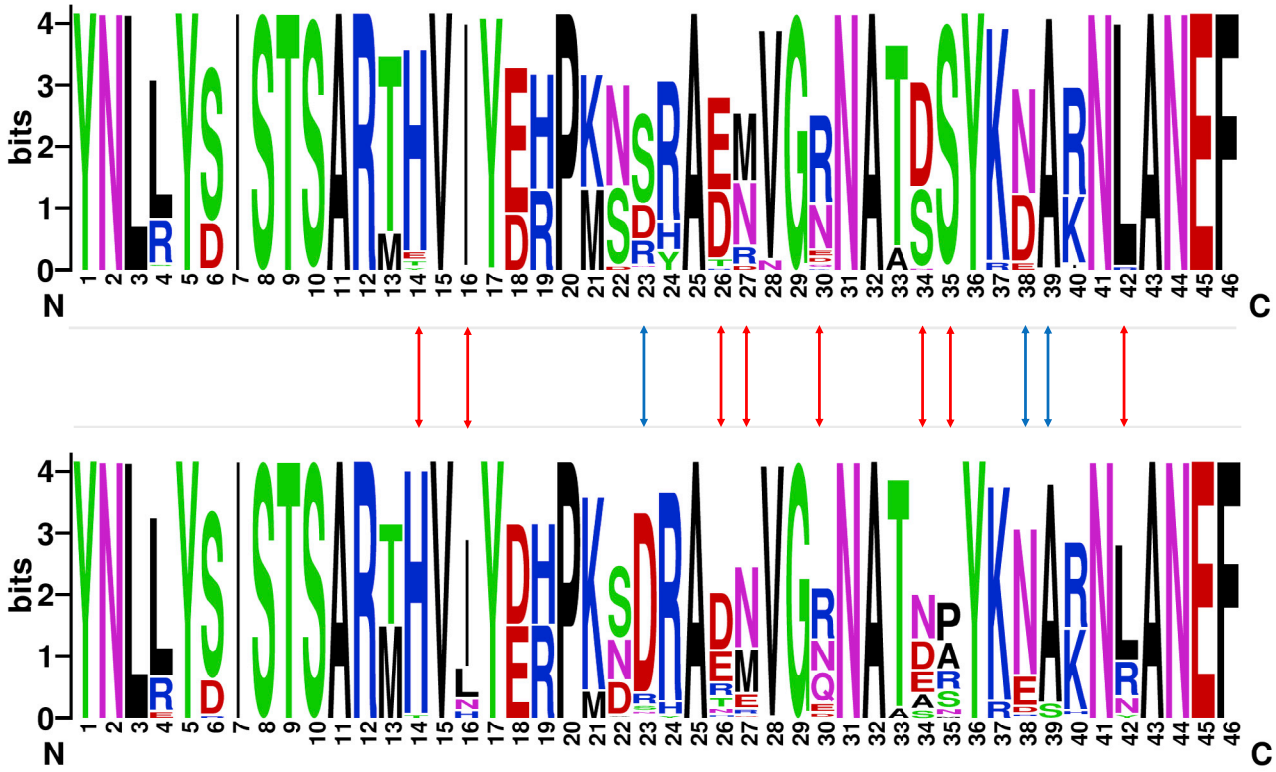

Top 100 affinity attenuating designs

(1) Tyr456, (2) Asn543, (3) Leu544, (4) Lys545, (5) Tyr546, (6) Ala547, (7) Ile548, (8) Ser549, (9) Lys551, (10) Arg553, (11) Ala554, (12) Arg555, (13) Thr556, (14) Val557, (15) Val560, (16) Ile589, (17) Trp617, (18) Asp618, (19) Tyr619, (20) Pro620, (21) Lys621, (22) Cys622, (23) Asp623, (24) Arg624, (25) Ala625, (26) Met626, (27) Arg631, (28) Val662, (29) Gly679, (30) Thr680, (31) Ser681, (32) Ala685, (33) Thr686, (34) Thr687, (35) Ala688, (36) Tyr689, (37) Ala690, (38) Asn691, (39) Ser692, (40) Phe694, (41) Asn695, (42) Leu758, (43) Ala762, (44) Asn790, (45) Glu811, (46) Phe812

Figure 3. Sequence logos showing the frequency of designed remdesivir-interacting residues

Sequence logos of the 100 top-scored affinity-attenuating versus affinity-enhancing designs generated from the ligand-based interface design of the remdesivir-bound nsp12-nsp7-nsp8-RNA complex are shown. The integers on the X axis represent corresponding native residues, and their identities are shown in the bottom panel. The "bits" represent the overall height of the stack in the Y axis with the sequence conservation at that position. The blue arrow shows residues that exhibited diverse mutations between the two groups but with fewer amino acids sampled, and the red arrow shows residues that experienced more diverse sequence variations between the two groups with a relatively higher number of sampled amino acids.

Intermolecular interactions and visualization of remdesivir-bound top-ranked affinity-enhancing and affinity-attenuating nsp12 designs

To compare how the top-scoring affinity-attenuating remdesivir-bound designs differ from the top-scoring affinity-enhancing designs, we visualized the various types of intermolecular interactions between them. The numbers of intermolecular interactions that determine these variations were also computed. The affinity-enhancing design formed 312 interactions, and the affinity-attenuating design formed only 291 interactions in total (Table 1). Proximal interactions, polar contacts, and aromatic contacts were the major interactions that governed the increased or decreased affinity between remdesivir and nsp12 (Figures 4A and 4B). A ligand interaction diagram between remdesivir and nsp12 for the affinity-enhancing and affinity-attenuating designs shows that the lack of a metal-ion bond and hydrogen bonds between remdesivir

Table 1. Detailed intermolecular interactions formed between remdesivir and nsp12 binding residues and between Molnupiravir and nsp12 binding residues in the top-scoring affinity-enhancing and affinity-attenuating designs

	Remdesivir-nsp12		Molnupiravir-nsp12	
Types of Interactions	Affinity-Enhancing Design1	Affinity-Attenuating Design1	Affinity-Enhancing Design1	Affinity-Attenuating Design1
Van der waals interactions	2	4	5	2
Proximal interactions	264	251	239	225
Polar contacts	14	11	10	9
Hydrogen bonds	5	5	6	2
Aromatic contacts	25	18	15	13
Hydrophobic contacts	2	2	4	3
Carbonyl interactions	0	0	2	0
Total number of interactions	312	291	281	254

and Ser687, Ser688, and Ser622 residues of nsp12 were the major contributors to lower binding affinity in the affinity-attenuating design (Figures 4C and 4D).

Comparative analysis between Molnupiravir-bound nsp12 designs and remdesivir-bound nsp12 designs

The antiviral drug Molnupiravir was docked into the remdesivir binding site of SARS-CoV-2 RdRp, and Molnupiravir and remdesivir shared several common interactions with nsp12, including hydrogen bonds with Asn691 and the U10 and U20 of the primer RNA. Molnupiravir also established a unique hydrogen bond with Ser759 (Figure 5A and 5B). Because Molnupiravir shared a significant number of similar interactions with remdesivir (Figure 5C), we performed a ligand-based interface design of Molnupiravir-binding site residues of nsp12 and found 53 contacts and interactions with nsp12 (excluding 12 RNA-interacting and catalytically important nsp12 residues). The identical design condition and methodology to those used in the remdesivir-based nsp12 design were employed, and 50,000 designs from the interface designs were computed for Rosetta total score, RMSD, interface delta, and sequence identity.

Similar to the remdesivir-bound nsp12 designs, we first sampled the 50,000 designs of Molnupiravir-bound nsp12 by computing the total scores versus the RMSD (Figure S3A). We also performed a control experiment in which we only repacked the same 53 residues of nsp12 and considered the designs that were poorer in total score and binding affinity. We found that the designs with higher energy also exhibited RMSDs far from the native (>0.75 Å). Our subsequent calculations of total score versus interface delta, which showed the binding affinity, demonstrated that the lower binding affinity designs retained relatively higher energies, and a substantial number of designs had lower binding affinity compared with the control group structures (Figure S3B). We analyzed and plotted the RMSD versus the interface delta of the designs and observed that the designs with significantly lower binding affinities for Molnupiravir were somewhat structurally disparate from the native structures (Figure S3C). More than half of the designs scored lower than the control group, which showed the effect of mutations in the Molnupiravir-binding site of nsp12. The final evaluation of the binding affinities compared with the sequence identity of the designs revealed similar characteristics to the remdesivir-binding nsp12 designs, in which only four residues were more prone to mutations (Figure S3D). This result suggests that a few residues of nsp12 from SARS-CoV-2 are more susceptible to mutations at the Molnupiravir-binding site and may develop resistance via beneficial mutations to avoid evolutionary and external pressure.

The 50,000 designs that were generated surrounding the Molnupiravir-binding site of nsp12 were classified as either affinity-enhancing or affinity-attenuating designs, similar to those designed surrounding the remdesivir-binding site of nsp12. The 53 interacting amino acid residues of the 100 top-scoring affinity-enhancing and affinity-attenuating designs from each group were analyzed. A mutational landscape

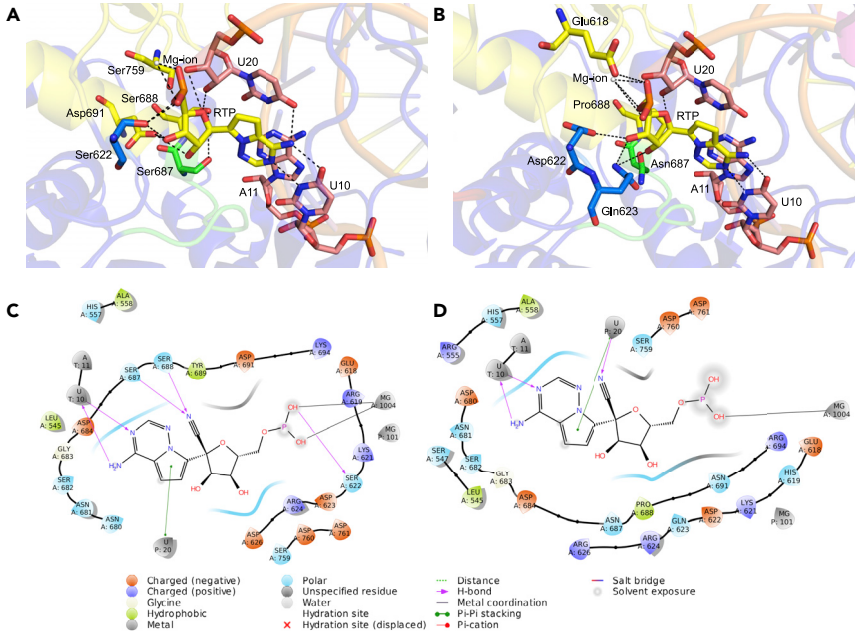

Figure 4. Key interactions and ligand interaction diagrams between remdesivir and the nsp12-nsp7-nsp8-RNA complex for the top-scoring affinity-enhancing and affinity-attenuating designs

Key intermolecular interactions between remdesivir and the nsp12-nsp7-nsp8-RNA complex for the top-scored (A) affinity-enhancing design and (B) affinity-attenuating design are shown. Interacting residues of corresponding nsp12 subdomains (green, blue, and yellow) and RNA bases (light pink) of remdesivir (yellow) are labeled and shown as stick models. The Mg^{2+} (gray sphere) coordinating the RTP is shown. Hydrogen bond interactions are shown as black dashes. 2D ligand interaction diagrams between remdesivir and the nsp12-nsp7-nsp8-RNA complex for the top-scored (C) affinity-enhancing design and (D) affinity-attenuating design are shown within a 6-Å distance. Various types of intermolecular interactions are labeled in the legend.

analysis revealed that residues Val560, Met626, and Phe694 exhibited diverse mutations between the two groups but with fewer amino acids sampled in these positions (Figure S4). Notably, some other residues, including Lys545, Ile589, Cys622, and Asn691, exhibited more diverse sequence variations between the two groups and with a relatively higher number of amino acids sampled (Figure S4). Only seven residue positions of nsp12 varied between the affinity-enhancing and affinity-attenuating designs compared with 11 residues in the remdesivir-bound nsp12 designs. This mutational landscape data between the affinity-attenuating and affinity-enhancing designs shows that remdesivir-binding sites of nsp12 had a higher number of mutations, and the Molnupiravir-binding site residues of nsp12 were relatively immune to mutation.

Our binding affinity calculations using PRODIGY-LIG for the Molnupiravir-bound designs showed that the designs exhibited binding affinities that ranged from −6.26 kcal/mol to −7.27 kcal/mol (Figure S5). With the decrease in the number of total contacts, the binding affinities were decreased. However, the difference in the binding affinity of the remdesivir-bound designs was higher (−1.34 kcal/mol) than that of the Molnupiravir-bound designs (−1.01 kcal/mol).

We visualized the various types of intermolecular interactions between the top-scoring affinity-enhancing designs of Molnupiravir and the top-scored affinity-attenuating designs of Molnupiravir. We found that the affinity-enhancing design formed 281 interactions, but the affinity-attenuating design formed only 254 interactions in total (Table 1). van der Waals interactions, proximal interactions, and hydrogen bonds were the major interactions that governed the increased or decreased affinity between Molnupiravir and nsp12. A ligand interaction diagram between Molnupiravir and nsp12 for the affinity-enhancing and affinity-attenuating designs clearly shows that the absence of a higher number of hydrogen bonds with Lys545 formed between nsp12 and Molnupiravir contributed to the lower binding affinity (Figure S6).

A comparison of nsp12 remdesivir-bound designs to the Molnupiravir-bound nsp12 designs suggested that Molnupiravir would be more effective in preventing the emergence of resistant mutations and against

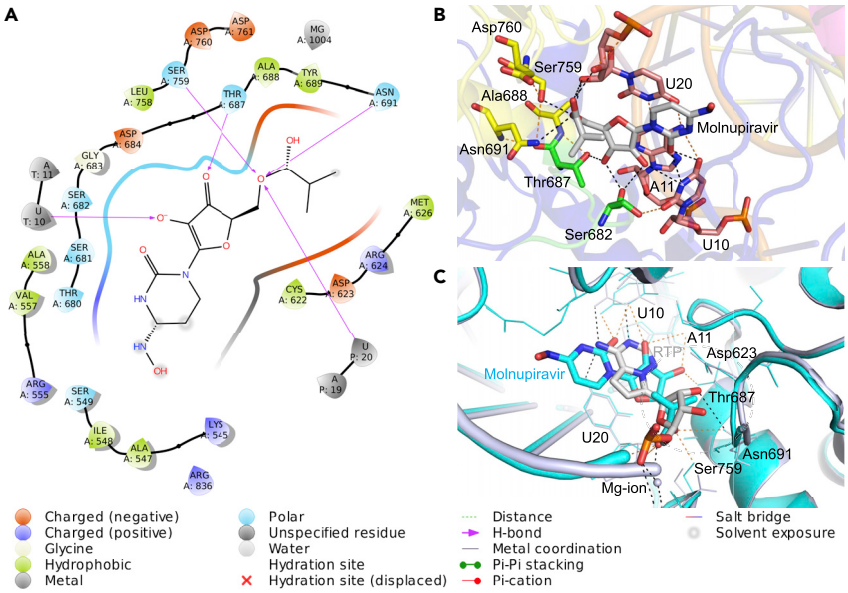

Figure 5. Interactions between Molnupiravir and the nsp12-nsp7-nsp8-RNA complex and its docked pose inside nsp12-nsp7-nsp8-RNA

(A) Ligand interaction diagram of Molnupiravir within a 6-Å distance of the nsp12-nsp7-nsp8 complex bound to the template-primer RNA is shown. The types of intermolecular interactions are labeled.

(B and C) (B) Interacting residues of corresponding nsp12 subdomains (green, blue, and yellow) and RNA bases (light pink) of Molnupiravir (gray) are labeled and shown as stick models. Hydrogen bond and salt bridge interactions are shown as black and orange dashes, respectively. (C) Structural superposition of the starting structure of the remdesivir-bound nsp12-nsp7-nsp8-RNA complex (gray) and the Molnupiravir-docked nsp12-nsp7-nsp8-RNA complex (cyan) is shown, where remdesivir is shown as a gray stick and Molnupiravir is shown as a cyan stick. The commonly interacting residues and RNA bases of remdesivir and Molnupiravir are shown as gray and cyan color lines, respectively and labeled. Hydrogen bond interactions for remdesivir and Molnupiravir are shown as black and orange dashes, respectively, all of which suggest a highly identical binding pose and conformation for remdesivir and Molnupiravir binding.

remdesivir-resistance strains. However, it is worth noting here that these results are not the sole explanation of why Molnupiravir is an effective inhibitor of the nsp12-V557L mutant, as other factors may play a role in conferring its efficacy; e.g., in addition to inhibiting viral RdRp, Molnupiravir exerts its antiviral effect through binding to many off-targets, and it also induces lethal mutagenesis by inducing deleterious mutations in the viral RNA (Sheahan et al., 2020).

Normal mode analysis and local flexibility of nsp12

We computed the normal modes of nsp12 of SARS-CoV-2 RdRp to understand which portions and sites of nsp12 undergo large-amplitude movements. Comparisons of these modes to our remdesivir-binding site designs of nsp12 are crucial to understanding the dynamics and flexibility of crucial nsp12 sites. First, our analysis of the displacement of each Cα atom for modes 1 to 6 revealed that although nsp12 exhibits interdomain motions, residues 400–750 were stable in some of the modes (Figure 6C). Second, our calculation of the square of the fluctuation of each Cα-atom calculated from the 200 lowest nontrivial modes and normalized showed that nsp12 residues 400–800 exhibited fewer fluctuations compared with other sites (Figure 6A). Third, our residue correlation analysis, which represented the correlated movement of the Cα atom in the nsp12 protein, showed that residues 450–780 of nsp12 undergo a highly correlated coupled motion (Figure 6B). Finally, our per-residue average B-factor analysis revealed the local flexibility and an overall domain motion of nsp12 (Figure 6D). All of these data suggest that nsp12 residues 450–780 are highly stable. These data correlated well with our design results, which showed that the remdesivir-bound nsp12 designs exhibited lower RMSDs and did not undergo large conformational changes even after mutations.

Intrinsic disorder predisposition in the nsp12 structure upon mutations

Next, we analyzed whether the intrinsic disorder predisposition of the nsp12 is changed due to the hotspot mutations, i.e., whether the mutations cause a transition from an ordered to a disordered region in nsp12. It

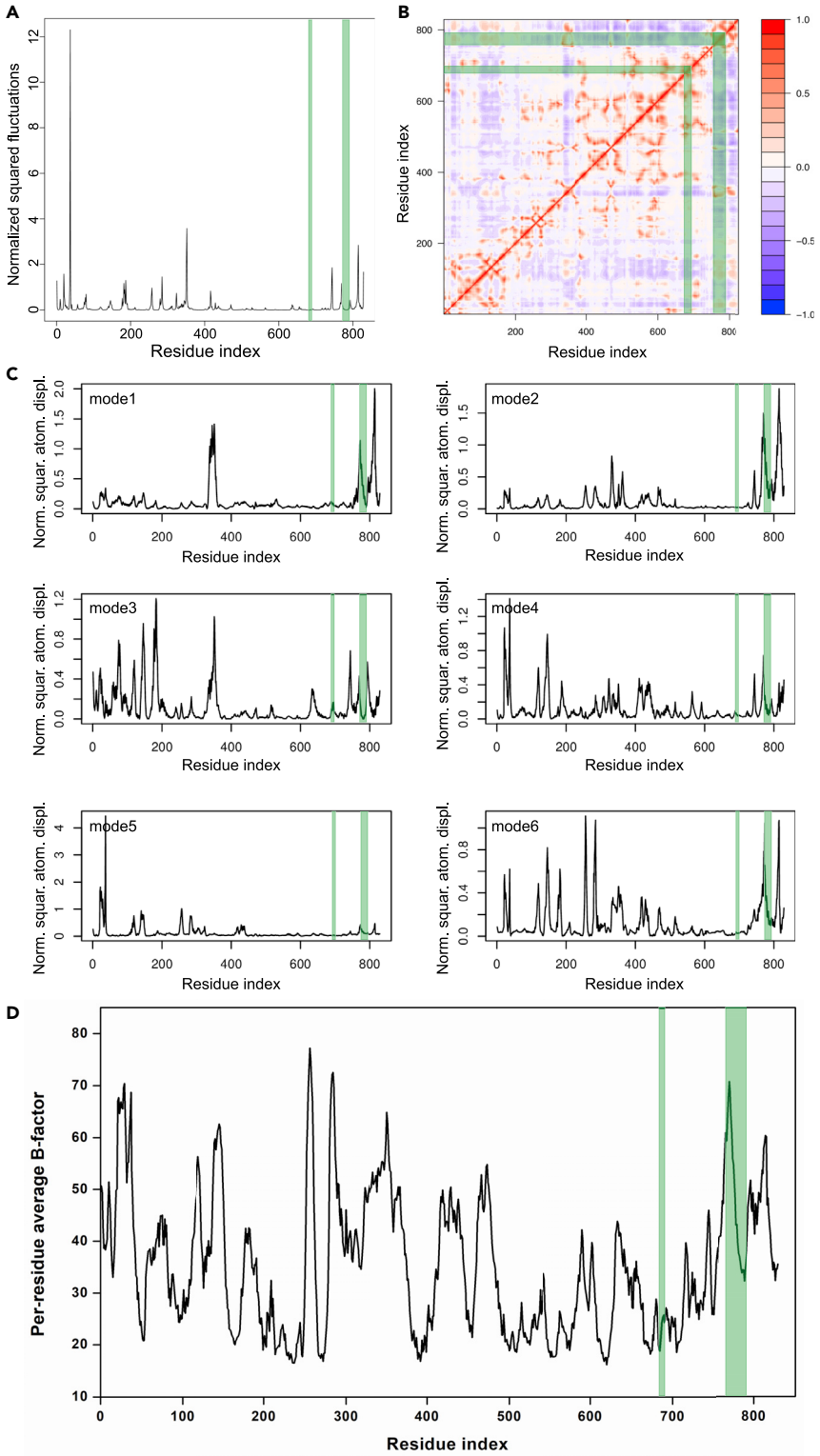

Figure 6. Normal mode analysis of nsp12

(A–D) (A) The normalized squared fluctuations and (B) the correlation matrix of nsp12 obtained from the normal mode analysis are shown. (C) The root-mean-square atomic displacements of nsp12 for six-modes are shown. (D) The per-residue average B-factor of nsp12 is shown to reflect the local flexibility. In all the figures, the remdesivir-binding regions of nsp12 are shown in the green box.

has been reported that the nsp12 of SARS-CoV-2 is highly structured with negligible levels of disorder (PPID <1%) (Giri et al., 2020). An overall predicted percentage of intrinsic disorder (PPID) was calculated for the wild-type nsp12 and the top 20 affinity-attenuating designs using five predictors. The mean PPID value for SARS-CoV-2 nsp12 was 0.84%. We also determined the mean PPID values of the top 20 affinity-attenuating designs and found that the values ranged between 0.72% and 1.08% (Table S1). Based on the overall level of intrinsic disorder content, proteins can be classified into three classes: highly ordered (PPID <10%), moderately disordered (PPID between 11% and 30%), and highly disordered (PPID $\geq$30%) (Lyngdoh et al., 2019; Uversky, 2013). All these data indicate negligible changes in the structural content in the affinity-attenuating designs, i.e., mutations did not induce any changes in the structural features of the affinity-attenuating designs.

DISCUSSION

Directed evolution is a powerful tool to generate and improve protein function via successive generations of random mutation, artificial selection, or screening (Romero and Arnold, 2009). During this process, the whole genome is subject to mutational events that can lead to increased fitness. At each instance of selection, changes in organismal fitness are directly linked to changes in enzyme stability and activity (Bloom et al., 2006). The population dynamics, therefore, reflect both the fitness and mutational landscape that can be traversed as selection proceeds (Couñago et al., 2006). At the molecular level, the complex interplay between immunological resistance mutations and the fitness landscape allows the development of antibody resistance across populations. SARS-CoV-2 has maintained a low mutation rate, which is attributed to the 3′-to-5′ exoribonuclease activity of the nsp14 protein, which helps maintain its replication fidelity (Shannon et al., 2020), suggesting that, at present, SARS-CoV-2 is not actively evolving, and there is no evidence of antigenic drift. However, with extended human-to-human transmission, SARS-CoV-2 could also acquire mutations with fitness advantages and immunological resistance (Callaway, 2020; Padhi and Tripathi, 2020). In addition, the viral load in a patient is very high (~100,000 viral copies per mL of saliva), which suggests that every possible mutation may develop over the course of infection (To et al., 2020). The evolutionary pressure due to drugs acts upon the existing viral population to favor a subpopulation that has a relatively better fitness in the new environment. This subpopulation may have a reduced genomic fidelity that results in the existence of a mutation that becomes favorable upon the addition of a drug. This results in a population shift such that this lower-fidelity population now becomes dominant.

RdRps catalyze the RNA template-dependent formation of phosphodiester bonds and facilitate virus replication and transcription. The nsp12 subunit of the RdRp of SARS-CoV-2 and that of SARS-CoV share a sequence identity of 96.4% and sequence similarity of 99.4%, which suggests that its function and mechanism of action are well conserved (Gao et al., 2020; Wu et al., 2020). RdRps are the primary targets for antiviral drug development against SARS-CoV-2, and several RdRp-targeting drugs, such as remdesivir, favipiravir, galidesivir, ribavirin, and penciclovir, are in testing stages (Agostini et al., 2018; Furuta et al., 2013; Morgenstern et al., 2005). Remdesivir is an investigational, broad-spectrum antiviral drug with activity against CoVs and other RNA viruses. It is being tested as a potential treatment for COVID-19 in multisite clinical trials, and it recently advanced to a phase 3 stage (Anonymous, 2020). Recent data from a randomized, double-blind, placebo-controlled trial of intravenous remdesivir have indicated that remdesivir was statistically superior to placebo in shortening the time to recovery in adults (Beigel et al., 2020). Remdesivir is a nucleoside analog that acts as an RdRp inhibitor and targets viral replication. Few naturally occurring mutations in RdRp that led to drug resistance were observed previously (Agostini et al., 2018; Goldhill et al., 2018; Young et al., 2003). Since its emergence in November 2019, several mutations in the RdRp of SARS-CoV-2 were reported. More than 870 unique nsp12 mutations have been reported and are listed in the CoV-GLUE database, and 41 of them are in the remdesivir-binding site (last accessed: 26 November 2020). A recent study identified mutation hotspots in SARS-CoV-2 (Pachetti et al., 2020). The results showed that viral strains with RdRp mutation had a median of 3-point mutations, and viral strains with no RdRp mutation had a median of 1 mutation. A mutation in position 14,408 of SARS-CoV-2 RdRp was associated with an increased mutation rate (Pachetti et al., 2020). Two nsp12 mutations (F480L and V557L) conferred an up to 5.6-fold resistance to SARS-CoV (Agostini et al., 2018), and these residues are conserved across all CoVs.

A detailed atomic-level understanding of RdRp interaction with remdesivir using robust molecular technologies could revolutionize the development of new therapies to fight COVID-19 in a highly specific and efficient manner. Thus, we designed 50,000 remdesivir-interacting nsp12 residues using high-throughput ligand-based interface design. We also docked the oral NHC prodrug (β-D-N^4-hydroxycytidine-5′-

isopropyl ester) Molnupiravir, which is similar to remdesivir because both drugs work by mimicking ribonucleosides, into the remdesivir-binding site of SARS-CoV-2 RdRp and designed 50,000 Molnupiravir-interacting nsp12 residues. Therefore, a total of 100,000 designs were devised and analyzed in detail. The most striking result was that even after designing 46 residues in the remdesivir-binding site of nsp12 and 53 residues in the Molnupiravir-binding site of nsp12, the designs retained an overall 97%–98% sequence identity, which suggests that SARS-CoV-2 attained resistance with very few mutations in nsp12. These highly mutation-prone residues/sites should be critically considered in the development of future therapeutics and during analyses of pandemic evolution. The affinity-attenuating designs showed lower remdesivir binding, which indicates that SARS-CoV-2 could develop remdesivir resistance via mutations at these residues. These hotspot residues would likely undergo selective mutations in the future to establish remdesivir and related drug resistance. Our design methodology mutated and rank-ordered specific remdesivir-resistance mutations of SARS-CoV, which highlights its accuracy and predictive ability. The normal mode analysis, residue correlation, and per-residue average B-factor analysis revealed the local flexibility and overall domain motion of nsp12 and suggested that residues 400–750 are mostly stable and undergo a highly correlated coupled motion. These results correlate well with our design results, in which remdesivir-bound nsp12 designs did not undergo large conformational changes and retained 97%–98% sequence identity even after mutations modulated the binding affinities with remdesivir and Molnupiravir. Compared with the 11 nsp12 residues in the remdesivir-bound designs, only 7 nsp12 residues varied in the Molnupiravir-bound designs. This result suggests that Molnupiravir is more effective in preventing the emergence of resistance mutations due to the restricted mutational landscape and partly explains why Molnupiravir is effective against remdesivir-resistant mutations. Our cohesive and comprehensive work highlights the hotspot residues of nsp12 that have the potential to undergo mutation to develop remdesivir resistance. Information on potential mutants could help clinicians adjust drug regimens to administer treatments earlier and more aggressively in higher-risk conditions.

We conclude that in the absence of detailed information on the evolutionary forces and the role of selection pressures, predicting how a virus may evolve is a challenging task, particularly during a nascent outbreak. The rapid availability of more SARS-CoV-2 genomes, most of which differ by one or few mutations, enables the accurate investigation into spread patterns. Genomic epidemiology-based analysis is being used to control the rapidly spreading SARS-CoV-2 outbreak (Mishra and Tripathi, 2021). Combined with the availability of more genomic data, our information on mutation repertoires is critical for predicting structural features that may guide the design of new drugs to counter resistant strains. Our prediction of the mutation repertoires complements research aimed at understanding and managing the mechanisms of SARS-CoV-2 drug resistance and COVID-19 pathogenesis and guides development strategies to deter future cross-species transmissions.

Limitations of the study

We acknowledge certain limitations in the current study. First, our Rosetta ligand-based interface design method (and scoring function) is set to design mutants with improved interface delta and therefore with increased binding affinity to remdesivir. However, typically, the remdesivir-resistant mutations are affinity-attenuating designs. To the best of our knowledge, at present, neither Rosetta nor any other programs have protocols to accurately score and predict affinity-attenuating designs to correlate with a drug resistance mutation. Nonetheless, Rosetta methodology remains the only useful design-based tool for mutational mapping and prediction of specific residues involved in enhancing or attenuating protein-ligand interaction. Therefore, to make sure that our Rosetta protocol captures the correct affinity-attenuating designs to correlate with remdesivir-resistant mutations, we carried out control experiments by taking the wild-type and a previously known remdesivir-resistant SARS-CoV mutation as controls. We argue that the affinity-attenuating designs representing the potential hotspot residues have a higher probability of undergoing selective mutations in the future to develop remdesivir and related drug-based resistance. Second, owing to the lack of structure of the RdRp-Molnupiravir complex, the exact structural information predicted from the docked complex of RdRp-Molnupiravir might not be precise; however, because remdesivir and Molnupiravir bind at the same position, the error might not be significant enough to impact our design results. Third, a fitness test to evaluate the nsp12 designs and validate it through functional assays would shed light on whether they are deleterious or not to the replication rate of the virus. Finally, biochemical experiments are necessary to validate the computational results to eventually establish the role of mutations in the gain or loss of interactions and to obtain a holistic view of the emergence of plausible remdesivir-resistant mutations.

Resource availability

Lead contact

Further information and requests for resources should be directed to and will be fulfilled by the Lead Contact, Timir Tripathi (timir.tripathi@gmail.com).

Materials availability

This study did not generate new unique reagents/material.

Data and code availability

All data produced or analyzed for this study are included in the published article, and additional information can be obtained by contacting the Lead Contact, Timir Tripathi (timir.tripathi@gmail.com).

METHODS

All methods can be found in the accompanying Transparent Methods supplemental file.

SUPPLEMENTAL INFORMATION

Supplemental Information can be found online at https://doi.org/10.1016/j.isci.2020.101992.

ACKNOWLEDGMENTS

The authors are grateful to Dr. Kam Y.J. Zhang (Laboratory for Structural Bioinformatics, RIKEN, Yokohama) for his continuous support and valuable suggestions for improving the manuscript. The authors acknowledge RIKEN ACCC for the Hokusai supercomputing resources. PS acknowledges the Science and Engineering Research Board, India, for support (EEQ/2018/000484).

AUTHOR CONTRIBUTIONS

AKP carried out all the design experiments, data generation, and analysis. RS performed the docking experiment. AKP and TT conceived the study and participated in its design and coordination. AKP, RS, PS, and TT analyzed the data and drafted the manuscript. All authors read and approved the final manuscript.

DECLARATION OF INTERESTS

The authors declare no competing interests.

Received: July 13, 2020
Revised: September 28, 2020
Accepted: December 21, 2020
Published: January 22, 2021

REFERENCES

Agostini, M.L., Andres, E.L., Sims, A.C., Graham, R.L., Sheahan, T.P., Lu, X., Smith, E.C., Case, J.B., Feng, J.Y., Jordan, R., et al. (2018). Coronavirus Susceptibility to the antiviral remdesivir (GS-5734) is Mediated by the viral polymerase and the proofreading exoribonuclease. mBio *9*, https://doi.org/10.1128/mBio.00221-18.

Ahn, D.G., Choi, J.K., Taylor, D.R., and Oh, J.W. (2012). Biochemical characterization of a recombinant SARS coronavirus nsp12 RNA-dependent RNA polymerase capable of copying viral RNA templates. Arch. Virol. *157*, 2095–2104, https://doi.org/10.1007/s00705-012-1404-x.

Alford, R.F., Leaver-Fay, A., Jeliazkov, J.R., O'Meara, M.J., DiMaio, F.P., Park, H., Shapovalov, M.V., Renfrew, P.D., Mulligan, V.K., Kappel, K., et al. (2017). The Rosetta all-atom energy function for macromolecular modeling and design. J. Chem. Theor. Comput. *13*, 3031–3048, https://doi.org/10.1021/acs.jctc.7b00125.

Andersen, K.G., Rambaut, A., Lipkin, W.I., Holmes, E.C., and Garry, R.F. (2020). The proximal origin of SARS-CoV-2. Nat. Med. *26*, 450–452, https://doi.org/10.1038/s41591-020-0820-9.

Anonymous. (2020). Multicenter, retrospective study of the effects of remdesivir in the treatment of severe covid-19 infections. https://ClinicalTrials.gov/show/NCT04365725.

Beigel, J.H., Tomashek, K.M., Dodd, L.E., Mehta, A.K., Zingman, B.S., Kalil, A.C., Hohmann, E., Chu, H.Y., Luetkemeyer, A., Kline, S., et al. (2020). Remdesivir for the treatment of covid-19 - final report. N. Engl. J. Med. *383*, 1813–1826, https://doi.org/10.1056/NEJMoa2007764.

Bloom, J.D., Labthavikul, S.T., Otey, C.R., and Arnold, F.H. (2006). Protein stability promotes evolvability. Proc. Natl. Acad. Sci. U S A *103*, 5869–5874, https://doi.org/10.1073/pnas.0510098103.

Callaway, E. (2020). Making sense of coronavirus mutations. Nature *585*, 174–177, https://doi.org/10.1038/d41586-020-02544-6.

Cao, Z.W., Han, L.Y., Zheng, C.J., Ji, Z.L., Chen, X., Lin, H.H., and Chen, Y.Z. (2005). Computer prediction of drug resistance mutations in proteins. Drug Discov. Today *10*, 521–529, https://doi.org/10.1016/s1359-6446(05)03377-5.

Couñago, R., Chen, S., and Shamoo, Y. (2006). In vivo molecular evolution reveals biophysical origins of organismal fitness. Mol. Cell *22*, 441–449, https://doi.org/10.1016/j.molcel.2006.04.012.

Cox, R.M., Wolf, J.D., and Plemper, R.K. (2020). Therapeutically administered ribonucleoside analogue MK-4482/EIDD-2801 blocks SARS-CoV-2 transmission in ferrets. Nat. Microbiol. https://doi.org/10.1038/s41564-020-00835-2.

Domingo, E., and Holland, J.J. (1997). RNA virus mutations and fitness for survival. Annu. Rev. Microbiol. *51*, 151–178, https://doi.org/10.1146/annurev.micro.51.1.151.

Duffy, S. (2018). Why are RNA virus mutation rates so damn high? PLoS Biol. *16*, e3000003, https://doi.org/10.1371/journal.pbio.3000003.

Fleishman, S.J., Leaver-Fay, A., Corn, J.E., Strauch, E.M., Khare, S.D., Koga, N., Ashworth, J., Murphy, P., Richter, F., Lemmon, G., et al. (2011). RosettaScripts: a scripting language interface to the Rosetta macromolecular modeling suite. PLoS One *6*, e20161, https://doi.org/10.1371/journal.pone.0020161.

Frey, K.M., Georgiev, I., Donald, B.R., and Anderson, A.C. (2010). Predicting resistance mutations using protein design algorithms. Proc. Natl. Acad. Sci. U S A *107*, 13707–13712, https://doi.org/10.1073/pnas.1002162107.

Furuta, Y., Gowen, B.B., Takahashi, K., Shiraki, K., Smee, D.F., and Barnard, D.L. (2013). Favipiravir (T-705), a novel viral RNA polymerase inhibitor. Antiviral. Res. *100*, 446–454, https://doi.org/10.1016/j.antiviral.2013.09.015.

Gao, Y., Yan, L., Huang, Y., Liu, F., Zhao, Y., Cao, L., Wang, T., Sun, Q., Ming, Z., Zhang, L., et al. (2020). Structure of the RNA-dependent RNA polymerase from COVID-19 virus. Science *368*, 779–782, https://doi.org/10.1126/science.abb7498.

Giri, R., Bhardwaj, T., Shegane, M., Gehi, B.R., Kumar, P., Gadhave, K., Oldfield, C.J., and Uversky, V.N. (2020). Understanding COVID-19 via comparative analysis of dark proteomes of SARS-CoV-2, human SARS and bat SARS-like coronaviruses. Cell. Mol. Life Sci. 1–34, https://doi.org/10.1007/s00018-020-03603-x.

Goldhill, D.H., Te Velthuis, A.J.W., Fletcher, R.A., Langat, P., Zambon, M., Lackenby, A., and Barclay, W.S. (2018). The mechanism of resistance to favipiravir in influenza. Proc. Natl. Acad. Sci. U S A *115*, 11613–11618, https://doi.org/10.1073/pnas.1811345115.

Gordon, C.J., Tchesnokov, E.P., Woolner, E., Perry, J.K., Feng, J.Y., Porter, D.P., and Gatte, M. (2020). Remdesivir is a direct-acting antiviral that inhibits RNA-dependent RNA polymerase from severe acute respiratory syndrome coronavirus 2 with high potency. J. Biol. Chem. *295*, 6785–6797, https://doi.org/10.1074/jbc.RA120.013679.

Guo, Y.R., Cao, Q.D., Hong, Z.S., Tan, Y.Y., Chen, S.D., Jin, H.J., Tan, K.S., Wang, D.Y., and Yan, Y. (2020). The origin, transmission and clinical therapies on coronavirus disease 2019 (COVID-19) outbreak - an update on the status. Mil. Med. Res. *7*, 11, https://doi.org/10.1186/s40779-020-00240-0.

Hadfield, J., Megill, C., Bell, S.M., Huddleston, J., Potter, B., Callender, C., Sagulenko, P., Bedford, T., and Neher, R.A. (2018). Nextstrain: real-time tracking of pathogen evolution. Bioinformatics *34*, 4121–4123, https://doi.org/10.1093/bioinformatics/bty407.

Kaufmann, K.W., and Meiler, J. (2012). Using RosettaLigand for small molecule docking into comparative models. PLoS One *7*, e50769, https://doi.org/10.1371/journal.pone.0050769.

Kirchdoerfer, R.N., and Ward, A.B. (2019). Structure of the SARS-CoV nsp12 polymerase bound to nsp7 and nsp8 co-factors. Nat. Commun. *10*, 2342, https://doi.org/10.1038/s41467-019-10280-3.

Lehmann, K.C., Gulyaeva, A., Zevenhoven-Dobbe, J.C., Janssen, G.M., Ruben, M., Overkleeft, H.S., van Veelen, P.A., Samborskiy, D.V., Kravchenko, A.A., Leontovich, A.M., et al. (2015). Discovery of an essential nucleotidylating activity associated with a newly delineated conserved domain in the RNA polymerase-containing protein of all nidoviruses. Nucleic Acids Res. *43*, 8416–8434, https://doi.org/10.1093/nar/gkv838.

Lu, R., Zhao, X., Li, J., Niu, P., Yang, B., Wu, H., Wang, W., Song, H., Huang, B., Zhu, N., et al. (2020). Genomic characterisation and epidemiology of 2019 novel coronavirus: implications for virus origins and receptor binding. Lancet *395*, 565–574, https://doi.org/10.1016/s0140-6736(20)30251-8.

Lyngdoh, D.L., Shukla, H., Sonkar, A., Anupam, R., and Tripathi, T. (2019). Portrait of the Intrinsically disordered side of the HTLV-1 proteome. ACS Omega *4*, 10003–10018, https://doi.org/10.1021/acsomega.9b01017.

Mishra, S.K., and Tripathi, T. (2021). One year update on the COVID-19 pandemic: where are we now? Acta Trop. *214*, 105778, https://doi.org/10.1016/j.actatropica.2020.105778.

Moretti, R., Bender, B.J., Allison, B., and Meiler, J. (2016). Rosetta and the design of ligand binding sites. Methods Mol. Biol. *1414*, 47–62, https://doi.org/10.1007/978-1-4939-3569-7_4.

Morgenstern, B., Michaelis, M., Baer, P.C., Doerr, H.W., and Cinatl, J., Jr. (2005). Ribavirin and interferon-beta synergistically inhibit SARS-associated coronavirus replication in animal and human cell lines. Biochem. Biophys. Res. Commun. *326*, 905–908, https://doi.org/10.1016/j.bbrc.2004.11.128.

Pachetti, M., Marini, B., Benedetti, F., Giudici, F., Mauro, E., Storici, P., Masciovecchio, C., Angeletti, S., Ciccozzi, M., Gallo, R.C., et al. (2020). Emerging SARS-CoV-2 mutation hot spots include a novel RNA-dependent-RNA polymerase variant. J. Transl. Med. *18*, 179, https://doi.org/10.1186/s12967-020-02344-6.

Padhi, A.K., and Tripathi, T. (2020). Can SARS-CoV-2 accumulate mutations in the S-protein to increase pathogenicity? ACS Pharmacol. Transl. Sci. *3*, 1023–1026, https://doi.org/10.1021/acsptsci.0c00113.

Reeve, S.M., Gainza, P., Frey, K.M., Georgiev, I., Donald, B.R., and Anderson, A.C. (2015). Protein design algorithms predict viable resistance to an experimental antifolate. Proc. Natl. Acad. Sci. U S A *112*, 749–754, https://doi.org/10.1073/pnas.1411548112.

Romero, P.A., and Arnold, F.H. (2009). Exploring protein fitness landscapes by directed evolution. Nat. Rev. Mol. Cell Biol. *10*, 866–876, https://doi.org/10.1038/nrm2805.

Shannon, A., Le, N.T., Selisko, B., Eydoux, C., Alvarez, K., Guillemot, J.C., Decroly, E., Peersen, O., Ferron, F., and Canard, B. (2020). Remdesivir and SARS-CoV-2: structural requirements at both nsp12 RdRp and nsp14 Exonuclease active-sites. Antivir. Res. *178*, 104793, https://doi.org/10.1016/j.antiviral.2020.104793.

Sheahan, T.P., Sims, A.C., Zhou, S., Graham, R.L., Pruijssers, A.J., Agostini, M.L., Leist, S.R., Schäfer, A., Dinnon, K.H., 3rd, Stevens, L.J., et al. (2020). An orally bioavailable broad-spectrum antiviral inhibits SARS-CoV-2 in human airway epithelial cell cultures and multiple coronaviruses in mice. Sci. Transl. Med. *12*, eabb5883, https://doi.org/10.1126/scitranslmed.abb5883.

Subissi, L., Posthuma, C.C., Collet, A., Zevenhoven-Dobbe, J.C., Gorbalenya, A.E., Decroly, E., Snijder, E.J., Canard, B., and Imbert, I. (2014). One severe acute respiratory syndrome coronavirus protein complex integrates processive RNA polymerase and exonuclease activities. Proc. Natl. Acad. Sci. U S A *111*, E3900–E3909, https://doi.org/10.1073/pnas.1323705111.

Tchesnokov, E.P., Feng, J.Y., Porter, D.P., and Gatte, M. (2019). Mechanism of inhibition of ebola virus RNA-dependent RNA polymerase by remdesivir. Viruses *11*, 326, https://doi.org/10.3390/v11040326.

te Velthuis, A.J., Arnold, J.J., Cameron, C.E., van den Worm, S.H., and Snijder, E.J. (2010). The RNA polymerase activity of SARS-coronavirus nsp12 is primer dependent. Nucleic Acids Res. *38*, 203–214, https://doi.org/10.1093/nar/gkp904.

To, K.K., Tsang, O.T., Leung, W.S., Tam, A.R., Wu, T.C., Lung, D.C., Yip, C.C., Cai, J.P., Chan, J.M., Chik, T.S., et al. (2020). Temporal profiles of viral load in posterior oropharyngeal saliva samples and serum antibody responses during infection by SARS-CoV-2: an observational cohort study. Lancet Infect. Dis. *20*, 565–574, https://doi.org/10.1016/S1473-3099(20)30196-1.

Uversky, V.N. (2013). A decade and a half of protein intrinsic disorder: biology still waits for physics. Protein Sci. *22*, 693–724, https://doi.org/10.1002/pro.2261.

Wu, F., Zhao, S., Yu, B., Chen, Y.-M., Wang, W., Song, Z.-G., Hu, Y., Tao, Z.-W., Tian, J.-H., Pei, Y.-Y., et al. (2020). A new coronavirus associated with human respiratory disease in China. Nature *579*, 265–269, https://doi.org/10.1038/s41586-020-2008-3.

Yin, W., Mao, C., Luan, X., Shen, D.D., Shen, Q., Su, H., Wang, X., Zhou, F., Zhao, W., Gao, M., et al. (2020). Structural basis for inhibition of the RNA-dependent RNA polymerase from SARS-CoV-2 by remdesivir. Science *368*, 1499–1504, https://doi.org/10.1126/science.abc1560.

Young, K.C., Lindsay, K.L., Lee, K.J., Liu, W.C., He, J.W., Milstein, S.L., and Lai, M.M. (2003). Identification of a ribavirin-resistant NS5B mutation of hepatitis C virus during ribavirin monotherapy. Hepatology *38*, 869–878, https://doi.org/10.1053/jhep.2003.50445.

Ziebuhr, J. (2005). The coronavirus replicase. Curr. Top. Microbiol. Immunol. *287*, 57–94, https://doi.org/10.1007/3-540-26765-4_3.

iScience, Volume *24*

Supplemental Information

High-throughput rational design of the remdesivir binding site in the RdRp of SARS-CoV-2: implications for potential resistance

Aditya K. Padhi, Rohit Shukla, Prakash Saudagar, and Timir Tripathi

SUPPLEMENTAL INFORMATION

High-Throughput Rational Design of the Remdesivir Binding Site in the RdRp of SARS-CoV-2: Implications for Potential Resistance

Aditya K. Padhi[1], Rohit Shukla[2], Prakash Saudagar[3*], and Timir Tripathi[4*#]

[1]Laboratory for Structural Bioinformatics, Center for Biosystems Dynamics Research, RIKEN, Yokohama, Kanagawa 230-0045, Japan

[2]Department of Biotechnology and Bioinformatics, Jaypee University of Information Technology, Waknaghat, Solan- 173234, India

[3]Department of Biotechnology, National Institute of Technology, Warangal- 506004, India

[4]Molecular and Structural Biophysics Laboratory, Department of Biochemistry, North-Eastern Hill University, Shillong- 793022, India

***Corresponding authors:**

timir.tripathi@gmail.com (T. Tripathi)

ps@nitw.ac.in (P. Saudagar)

#Lead Contact:

timir.tripathi@gmail.com (T. Tripathi)

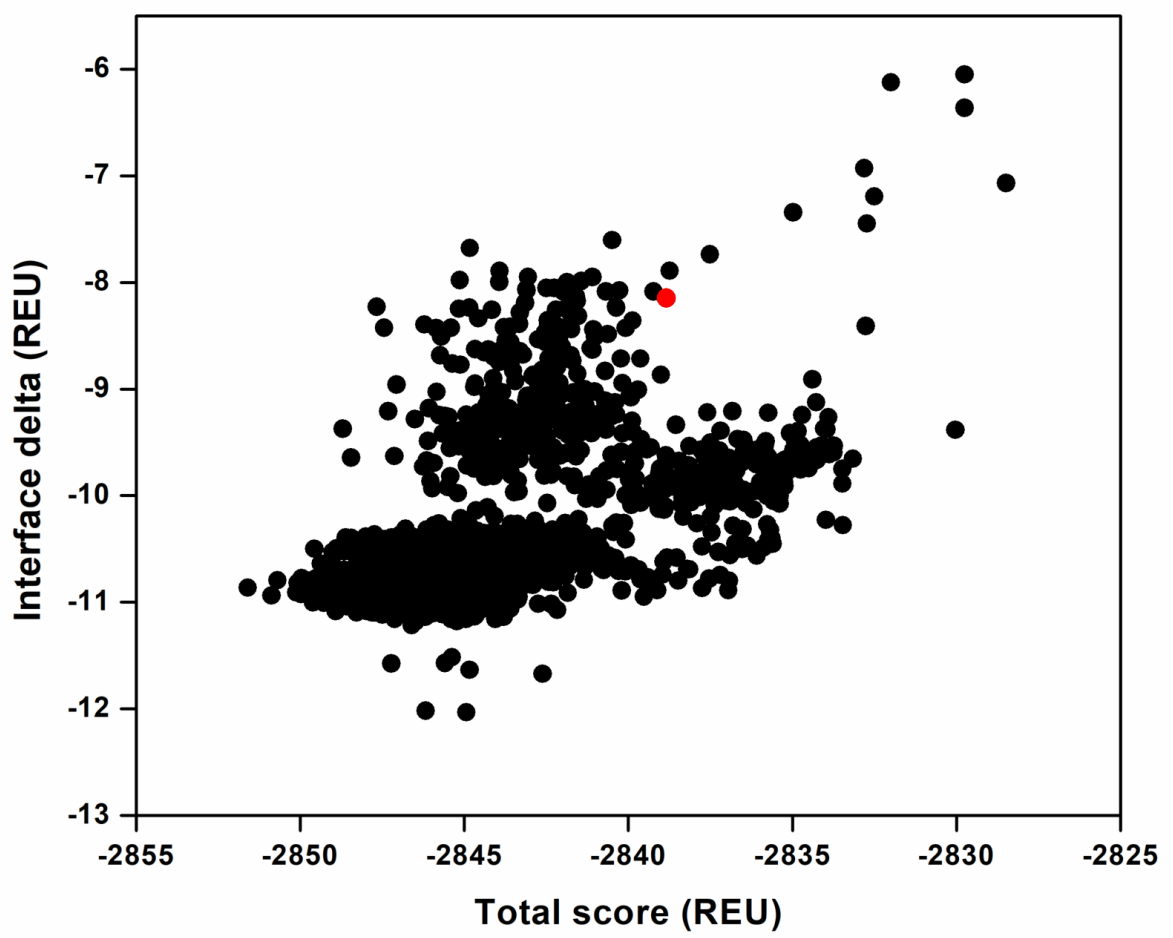

Figure S1. Rosetta total scores versus interface deltas of the computed designs in which only V557 was designed. The V557L design was among the low-affinity designs shown in red color. Figure S1. Validation of interface design protocol, Related to Figure 2.

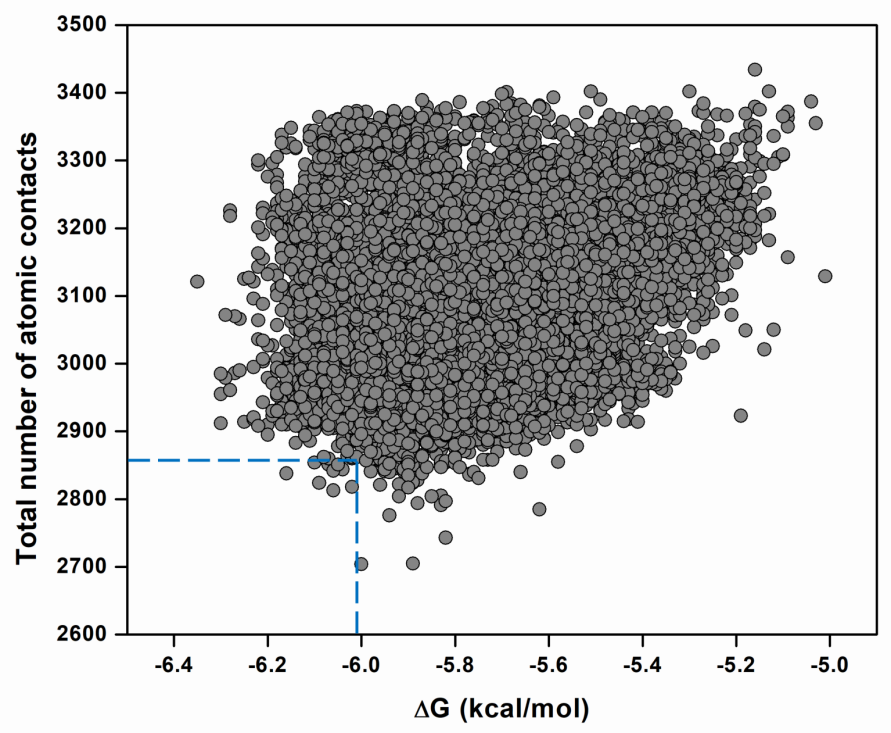

Figure S2. PRODIGY-LIG-derived binding affinities and atomic contacts. The binding affinities between remdesivir and the nsp12-nsp7-nsp8-RNA complex for the 50,000 generated designs are shown. The contact count represents the summation of (CC+CN+CO+CX+NN+NO+NX+OO+OX+XX) atomic contacts. Figure S2. PRODIGY-LIG derived binding affinities between remdesivir and designs, Related to Figure 3.

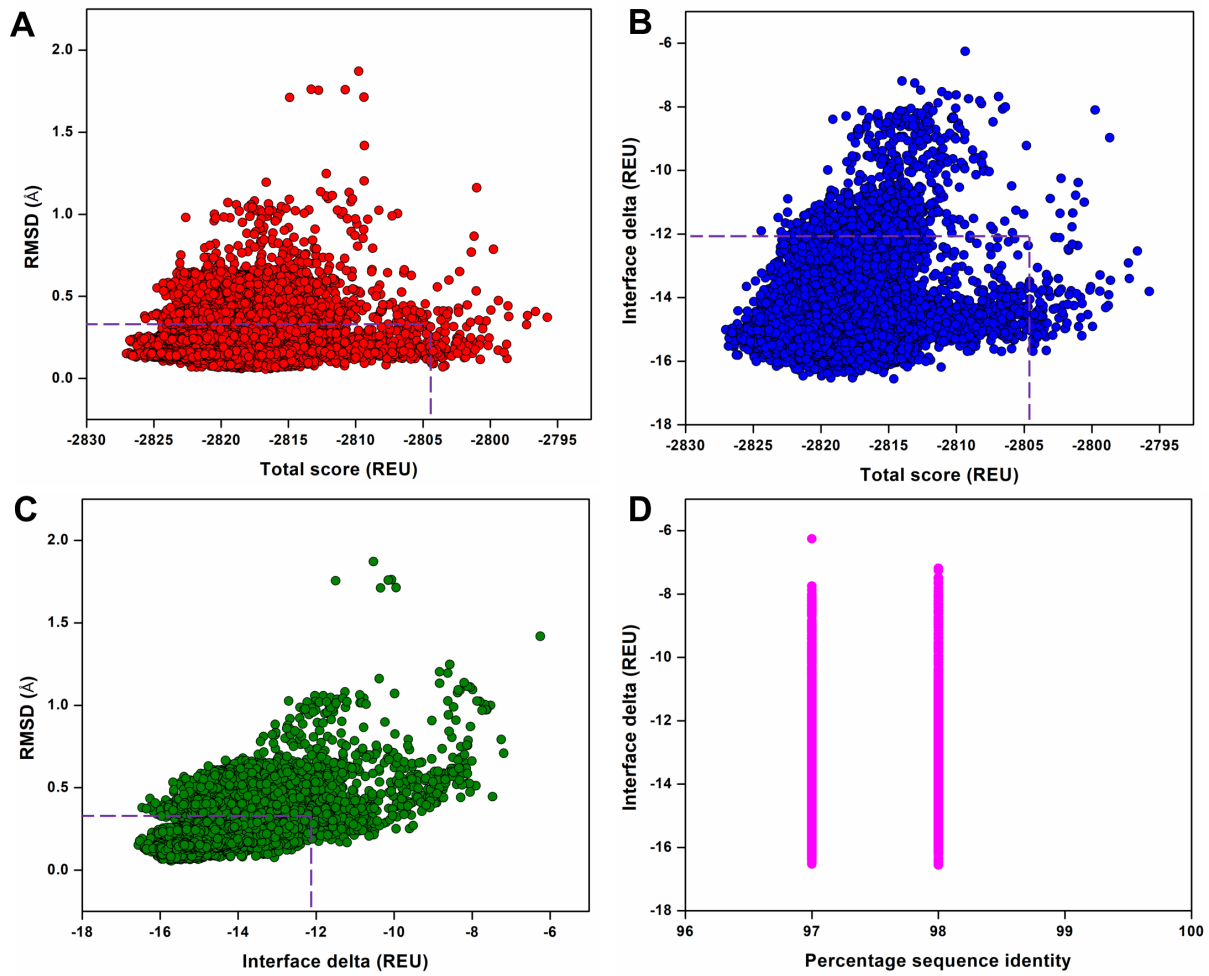

Figure S3. Structural and physicochemical parameters from the ligand-based Rosetta interface design experiment. (A) Rosetta total score versus RMSD of the 50,000 designs of the molnupiravir-bound nsp12-nsp7-nsp8 complex bound to the template-primer RNA complex obtained from the ligand-based interface design. (B) Rosetta total score versus interface delta representing the binding affinities of the designs between molnupiravir and the nsp12-nsp7-nsp8-RNA complex. (C) Interface delta versus RMSD of the designs, in which only the molnupiravir-interacting 53 residues were designed and the remaining residues were repacked. (D) Interface delta versus percentage sequence identity of the molnupiravir interacting residues of the nsp12-nsp7-nsp8-RNA complex showing the distribution of designs. In panels (A-C), the dotted boxes denote the control values in which the molnupiravir-interacting residues were only repacked and not designed. Figure S3. Physicochemical parameters of molnupiravir-binding designs, Related to Figure 2.

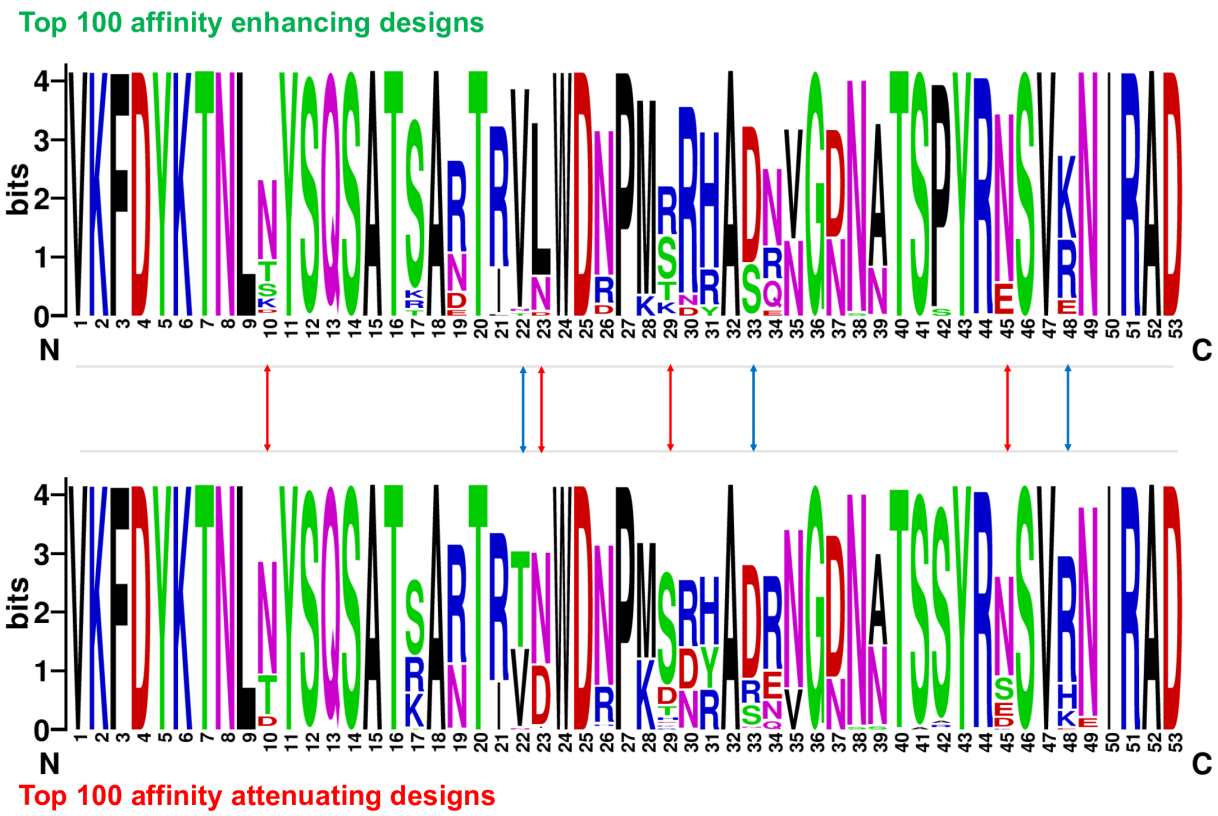

(1) Val410, (2) Lys411, (3) Phe440, (4) Asp452, (5) Tyr456, (6) Lys500, (7) Thr540, (8) Asn543, (9) Leu544, (10) Lys545, (11) Tyr546, (12) Ala547, (13) Ile548, (14) Ser549, (15) Ala550, (16) Lys551, (17) Arg553, (18) Ala554, (19) Arg555, (20) Thr556, (21) Val557, (22) Val560, (23) Ile589, (24) Trp617, (25) Asp618, (26) Tyr619, (27) Pro620, (28) Lys621, (29) Cys622, (30) Asp623, (31) Arg624, (32) Ala625, (33) Met626, (34) Arg631, (35) Val662, (36) Gly679, (37) Thr680, (38) Ser681, (39) Ala685, (40) Thr686, (41) Thr687, (42) Ala688, (43) Tyr689, (44) Ala690, (45) Asn691, (46) Ser692, (47) Val693, (48) Phe694, (49) Asn695, (50) Ile757, (51) Leu758, (52) Ala762, (53) Asp845

Figure S4. Sequence logos showing the frequency of the designed molnupiravir-interacting residues. Sequence logos of the 100 top-scoring affinity-enhancing versus affinity-attenuating designs generated from the ligand-based interface design of the molnupiravir-bound nsp12-nsp7-nsp8-RNA complex are shown. The integers on the X-axis represent corresponding native residues, and their identities are shown in the bottom panel. The 'bits' represent the overall height of the stack in the Y-axis with the sequence conservation at that position. The blue arrow shows residues that exhibited diverse mutations between the two groups but with fewer amino acids sampled, and the red arrow shows residues that experienced more diverse sequence variations between the two groups with a relatively higher number of sampled amino acids. Figure S4. Sequence diversity of molnupiravir-binding designs, Related to Figure 3.

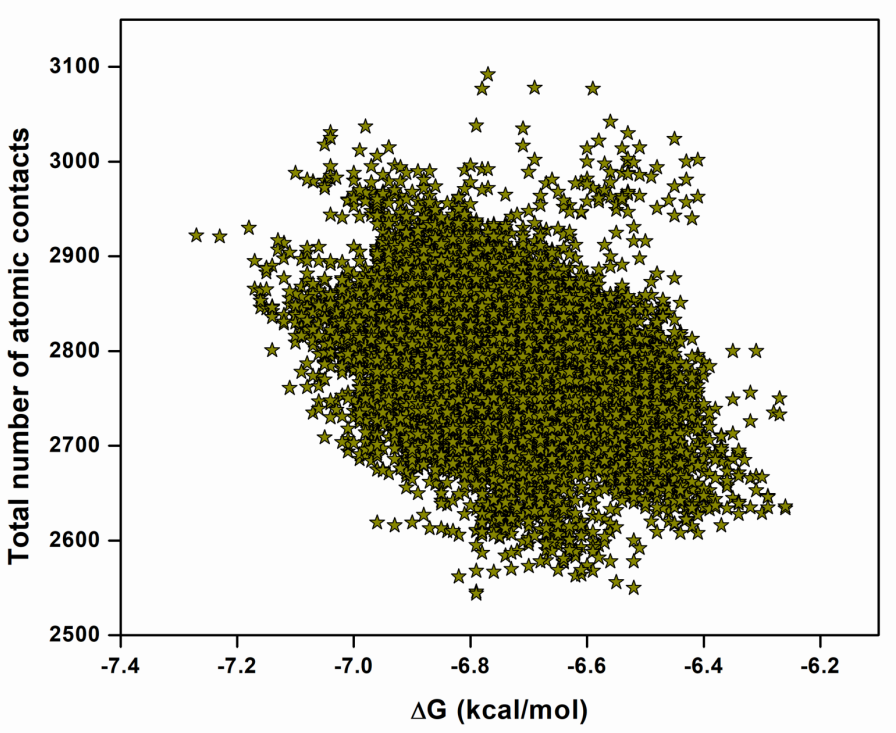

Figure S5. PRODIGY-LIG-derived binding affinities and atomic contacts. The binding affinities between molnupiravir and the nsp12-nsp7-nsp8-RNA complex for the 50,000 generated designs are shown. The contact count represents the summation of (CC+CN+CO+CX+NN+NO+NX+OO+OX+XX) atomic contacts. Figure S5. PRODIGY-LIG derived binding affinities between molnupiravir and designs, Related to Figure 5.

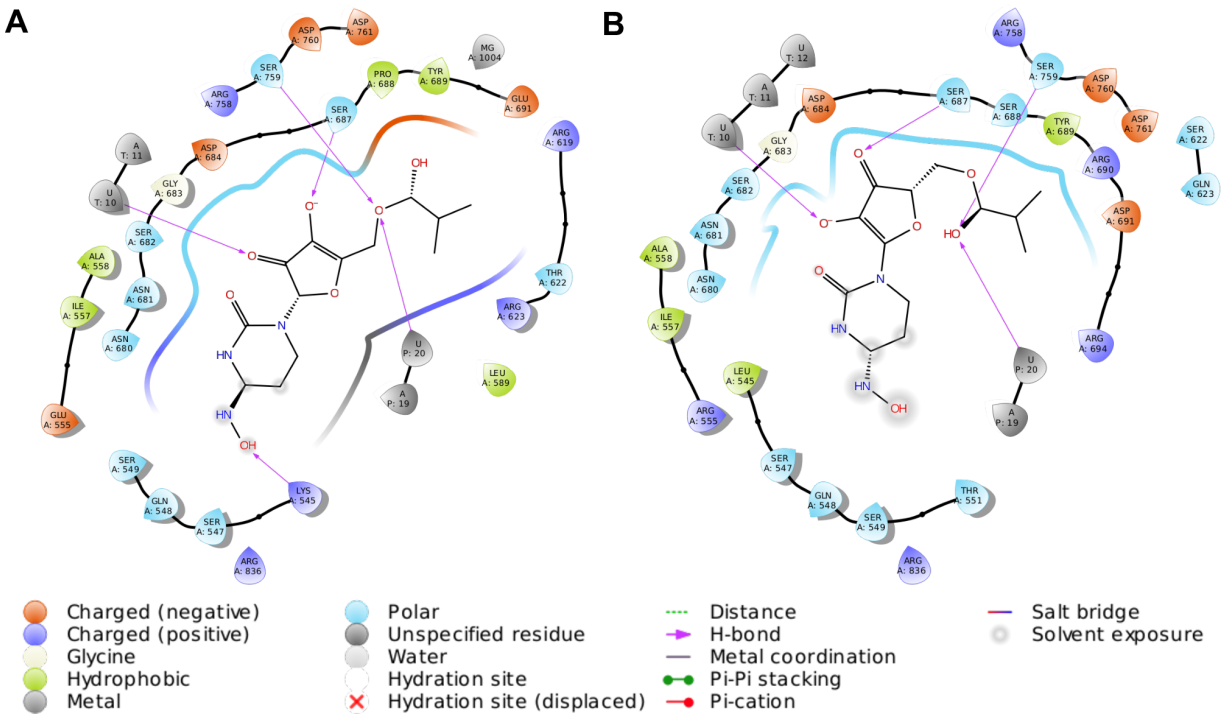

Figure S6. Ligand interaction diagrams between molnupiravir and the nsp12-nsp7-nsp8-RNA complex for the top-scoring affinity-enhancing and affinity-attenuating designs. 2D ligand interaction diagrams between molnupiravir and the nsp12-nsp7-nsp8-RNA complex for the top-scoring (A) affinity-enhancing design and (B) affinity-attenuating design are shown within a 6-Å distance. Various types of intermolecular interactions are labeled in legends. Figure S6. Molnupiravir interactions in the affinity-enhancing and affinity-attenuating designs, Related to Figures 4 and 5.

Supplementary Table S1. Predicted percentage of intrinsic disorder (PPID) of the wild-type and the top 20 affinity-attenuating designs. Supplementary Table S1. Percentage intrinsic disorder of the designs, Related to Figures 2 and 3.

Protein Name	$PPID_{VLXT}$ (%)	$PPID_{VSL2}$ (%)	$PPID_{IUPred\ Long}$ (%)	$PPID_{IUPred\ Short}$ (%)	$PPID_{Disopred}$ (%)	$PPID_{Mean}$ (%)
Wild-type	4.46	4.22	0.24	0.08	1.08	0.84
>use_000226	4.46	5.79	1.08	1.20	2.41	0.84
>use_000753	7.50	5.90	1.08	1.32	3.37	1.08
>use_002159	4.46	6.03	1.08	1.20	1.32	0.72
>use_003729	5.91	6.39	1.08	1.20	0.48	0.84
>use_013234	6.75	6.03	0.84	1.20	0.96	0.84
>use_017839	7.72	6.27	1.20	1.32	2.41	0.96
>use_018383	5.91	5.79	1.08	1.20	1.32	0.84
>use_020421	5.18	5.91	1.08	0.96	1.80	0.72
>use_024461	5.54	6.39	0.84	1.20	1.20	0.84
>use_026183	7.47	5.66	1.08	1.20	2.65	0.72
>use_028850	7.72	5.54	1.08	0.96	1.80	0.72
>use_032323	7.35	5.54	0.84	1.20	0.96	0.72
>use_033485	5.54	5.79	0.84	1.20	1.80	0.84
>use_036359	6.39	6.15	1.08	1.08	1.80	0.84
>use_040108	7.47	5.79	1.08	1.20	2.29	0.72
>use_048390	7.59	6.63	0.96	0.96	1.80	0.72
>use_049174	6.75	5.79	0.96	1.20	0.96	0.72
>use_051902	7.23	5.79	1.08	1.32	3.61	1.08
>use_056413	7.84	5.66	0.84	0.96	2.17	0.72
>use_062231	7.96	6.27	1.20	1.20	1.08	0.84

TRANSPARENT METHODS

Identification of interacting residues between nsp12 and the triphosphate form of remdesivir (RTP)

The cryo-EM structure of the RNA-dependent RNA polymerase from SARS-CoV-2 (PDB ID: 7BV2) consists of a nsp12-nsp7-nsp8 complex bound to the template-primer RNA and triphosphate form of RTP (Yin et al., 2020). These data were retrieved from the RCSB Protein Data Bank and subsequently used to obtain the key interactions and contacts between nsp12 and remdesivir. A total of 56 residues from nsp12 interacted with remdesivir.

Molecular docking of molnupiravir to the nsp12-nsp7-nsp8 complex bound to the template-primer RNA and triphosphate form of remdesivir (RTP)

Molnupiravir is an orally bioavailable NHC prodrug (β-D-N^4-hydroxycytidine-5′-isopropyl ester) that is similar to remdesivir, and both drugs work by mimicking ribonucleosides (Sheahan et al., 2020). Therefore, molnupiravir was docked into the remdesivir binding site of the RNA-dependent RNA polymerase of SARS-CoV-2. Molecular docking was performed using AutoDock Tools to dock the molnupiravir into the nsp12 binding cavity, in which it exerts its antiviral action via the introduction of copying errors during viral RNA replication (Huey et al., 2007; Morris et al., 1998). The nsp12-nsp7-nsp8 complex included the RNA and Mg^{2+} catalytic ions. PDB ID: 7BV2 is co-crystallized with remdesivir. The same binding grid was selected for the molnupiravir docking studies. The protein and ligands were prepared using the MGL tools. Hydrogens and Kollman charges were added to the protein, and hydrogen and Gaisteger charges were added to molnupiravir for preparation. The grid was set as X=42, Y=46, and Z=52 with 0.375-Å grid spacing. The protein and ligand were docked, and 100 binding poses were generated for the analysis. The best binding poses that laid well in the binding cavity and showed interactions with the key catalytic residues were selected for further analysis. The interactions between the complex and ligands were identified. A total of 65 residues from nsp12 interacted with molnupiravir.

Structural refinement of remdesivir- and molnupiravir-bound nsp12-nsp7-nsp8 in complex with template-primer RNA for Rosetta ligand-based interface design

The crystal structure of remdesivir-bound nsp12-nsp7-nsp8 and the molnupiravir-bound nsp12-nsp7-nsp8 in complex with template-primer RNA were first optimized using Schrödinger Maestro (Schrödinger Release 2016–4: Maestro, Schrödinger, New York). The parameters for remdesivir and molnupiravir were not available *a priori* for Rosetta-compatible forcefield. Therefore, the appropriate charges were added, and parameters for remdesivir and molnupiravir were generated. The resulting complexes with remdesivir and molnupiravir were used for structural refinement by Rosetta relax, which is the main protocol for all-atom refinement of structures in the Rosetta forcefield (Alford et al., 2017). Ten models were generated for each design group in this step, namely, the remdesivir-bound nsp12-nsp7-nsp8-template-primer RNA and molnupiravir-bound nsp12-nsp7-nsp8-template-primer RNA. The full atom-relaxed structures from each group with the lowest energy were used for subsequent ligand-based interface design experiments. The catalytically critical Mg^{2+} ions were retained in all of the refinement and subsequent design steps.

Ligand-based interface design and binding affinity calculation

Rosetta macromolecular modeling suite was used to perform the ligand-based interface design experiments (Moretti et al., 2016). The nsp12 was redesigned with allowed backbone flexibility using Rosetta's full-atom scoring function in the remdesivir- and molnupiravir-bound nsp12-nsp7-nsp8-template-primer RNA-bound structures. For the remdesivir-wrapped nsp12-nsp7-nsp8-template-primer RNA-bound structure, 46 residues of nsp12 that are known to interact with remdesivir were designed with 19 other amino acids, and 53 residues of nsp12 were designed to have intermolecular contacts with molnupiravir for the molnupiravir-bound nsp12-nsp7-nsp8-template-primer RNA-bound structure. During these design experiments, all of the other residues of nsp12, nsp7, and nsp8 were allowed to repack without design. A total of 100,000 designs composed of remdesivir- and molnupiravir-bound complexes were generated. A modified RosettaScripts was used to design the interface residues of nsp12 in complex with remdesivir and molnupiravir that considered a small movement of the backbone of nsp12

to avoid steric clashes with ligands upon the introduction of mutations (Fleishman et al., 2011). The designs were sampled using Monte-Carlo-simulated annealing in the Rosetta all-atom forcefield. For a comprehensive understanding of the structural and residue-specific changes of nsp12 upon interaction with remdesivir and molnupiravir, the Rosetta total score, root mean square deviation (RMSD) from the starting structure, Rosetta interface delta (representing the binding affinity between the designed nsp12 with remdesivir and molnupiravir), and the percentage sequence identity from the starting sequence were obtained.

Validating the design protocol on remdesivir-resistant nsp12 mutants of SARS-CoV

To test the accuracy and reliability of our ligand-based Rosetta interface design protocol, we considered a previously reported remdesivir-resistant mutant of SARS-CoV, V557L,, in which Val557 is a remdesivir-interacting residue of nsp12 (Sheahan et al., 2020). During this step, the Val557 residue was designed with the 19 other amino acids, but the remaining nsp12 residues were allowed to repack without further design. A total of 5000 designs were generated at the 557^{th} position and analyzed to monitor the highly prevalent designed residues with their corresponding scores and rankings.

Occurrence of mutations in top-ranked affinity-enhanced and affinity-attenuated designs

The type and frequency of designed amino acids in the 46 and 53 nsp12-interacting residues of remdesivir and molnupiravir, respectively, from the top-ranked affinity-enhanced and affinity-attenuated designs were obtained and plotted using WebLogo, which graphically represents the multiple sequence alignment of an amino acid profile (Crooks et al., 2004). The residue index is shown in the X-axis of these plots, and the sequence conservation of an amino acid at that position is shown on the Y-axis. The height of symbols within the stack in each plot indicates the relative frequency of a specific amino acid at that position.

Binding affinity calculation of remdesivir- and molnupiravir-bound nsp12 designs using PRODIGY-LIG

The 100,000 remdesivir- and molnupiravir-bound nsp12 structures generated using Rosetta ligand-based interface designs were subjected to the calculation of the binding affinities using PRODIGY-LI (PROtein binDIng enerGY prediction - LIGands), which is a structure-based method for the prediction of binding affinity in protein-ligand complexes (Kurkcuoglu et al., 2018; Vangone et al., 2019). A 3D model of the design with the bound ligand was supplied, and the binding affinity was computed. From the Rosetta-designed structures, the binding affinity (ΔG) and the contact counts were obtained for analysis. A detailed decomposition of intermolecular contacts was obtained for the top five affinity-enhancing and affinity-attenuating designs for the remdesivir- and molnupiravir-bound nsp12 structures.

Calculation of intermolecular interactions between remdesivir- and molnupiravir-bound nsp12 designs in the affinity-enhancing and affinity-attenuating mutants

The intermolecular interactions between top-ranked affinity-enhancing and affinity-attenuating remdesivir-nsp12 and molnupiravir-nsp12 designs were obtained using the Arpeggio web-server (Jubb et al., 2017). The total number of interactions obtained represents the sum of the number of van der Waals, proximal, polar contacts, hydrogen bonds, aromatic contacts, hydrophobic contacts, and carbonyl interactions.

Interaction diagrams between remdesivir-nsp12 and molnupiravir-nsp12 designs

The 2D-ligand interaction diagrams showing the various types of intermolecular interactions between remdesivir-nsp12 and molnupiravir-nsp12 top-ranked affinity-enhancing and affinity-attenuating designs were obtained using Schrödinger Maestro (Schrödinger Release 2016–4: Maestro, Schrödinger, New York). A distance up to 6 Å from the ligand molecule was considered when constructing the interaction diagrams.

Normal mode analysis of the RdRp subunit nsp12

The normal mode analysis, deformation energies of each mode, calculation of normalized squared atomic displacements, normalized squared fluctuations, and the correlation matrix of nsp12 were calculated using WEBnm@ server (Hollup et al., 2005; Tiwari et al., 2014).

Prediction of the intrinsic disorder propensity

To determine the intrinsic disorder propensity of the wild-type and the top 20 affinity-attenuating designs, five predictors were used, namely, PONDR VL-XT, PONDR VSL2, IUPred (Long and Short), and DISOPRED (Deng et al., 2012; Dosztányi et al., 2010). The predicted percent of intrinsic disorder (PPID) in a query protein was calculated from the outputs of all five predictors.

SUPPLEMENTAL REFERENCES

Alford, R.F., Leaver-Fay, A., Jeliazkov, J.R., O'Meara, M.J., DiMaio, F.P., Park, H., Shapovalov, M.V., Renfrew, P.D., Mulligan, V.K., Kappel, K., et al. (2017). The Rosetta All-Atom Energy Function for Macromolecular Modeling and Design. J Chem Theory Comput. 13(6), 3031-3048. Published online 2017/04/22 DOI: 10.1021/acs.jctc.7b00125.

Crooks, G.E., Hon, G., Chandonia, J.M., and Brenner, S.E. (2004). WebLogo: a sequence logo generator. Genome Res. 14(6), 1188-1190. Published online 2004/06/03 DOI: 10.1101/gr.849004.

Deng, X., Eickholt, J., and Cheng, J. (2012). A comprehensive overview of computational protein disorder prediction methods. Mol Biosyst. 8(1), 114-121. Published online 2011/08/30 DOI: 10.1039/c1mb05207a.

Dosztányi, Z., Mészáros, B., and Simon, I. (2010). Bioinformatical approaches to characterize intrinsically disordered/unstructured proteins. Brief Bioinform. 11(2), 225-243. Published online 2009/12/17 DOI: 10.1093/bib/bbp061.

Fleishman, S.J., Leaver-Fay, A., Corn, J.E., Strauch, E.M., Khare, S.D., Koga, N., Ashworth, J., Murphy, P., Richter, F., Lemmon, G., et al. (2011). RosettaScripts: a scripting language interface to the Rosetta macromolecular modeling suite. PLoS One. 6(6), e20161. Published online 2011/07/07 DOI: 10.1371/journal.pone.0020161.

Hollup, S.M., Salensminde, G., and Reuter, N. (2005). WEBnm@: a web application for normal mode analyses of proteins. BMC Bioinformatics. 6(1), 52. DOI: 10.1186/1471-2105-6-52.

Huey, R., Morris, G.M., Olson, A.J., and Goodsell, D.S. (2007). A semiempirical free energy force field with charge-based desolvation. J Comput Chem. 28(6), 1145-1152. Published online 2007/02/03 DOI: 10.1002/jcc.20634.

Jubb, H.C., Higueruelo, A.P., Ochoa-Montaño, B., Pitt, W.R., Ascher, D.B., and Blundell, T.L. (2017). Arpeggio: A Web Server for Calculating and Visualising Interatomic Interactions in Protein Structures. J Mol Biol. 429(3), 365-371. Published online 2016/12/15 DOI: 10.1016/j.jmb.2016.12.004.

Kurkcuoglu, Z., Koukos, P.I., Citro, N., Trellet, M.E., Rodrigues, J., Moreira, I.S., Roel-Touris, J., Melquiond, A.S.J., Geng, C., Schaarschmidt, J., et al. (2018). Performance of HADDOCK and a simple contact-based protein-ligand binding affinity predictor in the D3R Grand Challenge 2. J Comput Aided Mol Des. 32(1), 175-185. Published online 2017/08/24 DOI: 10.1007/s10822-017-0049-y.

Moretti, R., Bender, B.J., Allison, B., and Meiler, J. (2016). Rosetta and the Design of Ligand Binding Sites. Methods Mol Biol. 1414, 47-62. Published online 2016/04/21 DOI: 10.1007/978-1-4939-3569-7_4.

Morris, G.M., Goodsell, D.S., Halliday, R.S., Huey, R., Hart, W.E., Belew, R.K., and Oslon, A.J. (1998). Automated docking using a Lamarckian genetic algorithm and an empirical binding free energy function. J Comput Chem. 19, 1639–1662.

Sheahan, T.P., Sims, A.C., Zhou, S., Graham, R.L., Pruijssers, A.J., Agostini, M.L., Leist, S.R., Schäfer, A., Dinnon, K.H., 3rd, Stevens, L.J., et al. (2020). An orally bioavailable broad-spectrum antiviral inhibits SARS-CoV-2 in human airway epithelial cell cultures and multiple coronaviruses in mice. Sci Transl Med. 12(541), eabb5883. Published online 2020/04/08 DOI: 10.1126/scitranslmed.abb5883.

Tiwari, S.P., Fuglebakk, E., Hollup, S.M., Skjærven, L., Cragnolini, T., Grindhaug, S.H., Tekle, K.M., and Reuter, N. (2014). WEBnm@ v2.0: Web server and services for comparing protein flexibility. BMC Bioinformatics. 15(1), 427. DOI: 10.1186/s12859-014-0427-6.

Vangone, A., Schaarschmidt, J., Koukos, P., Geng, C., Citro, N., Trellet, M.E., Xue, L.C., and Bonvin, A. (2019). Large-scale prediction of binding affinity in protein-small ligand complexes: the PRODIGY-LIG web server. Bioinformatics. 35(9), 1585-1587. Published online 2019/05/06 DOI: 10.1093/bioinformatics/bty816.

Yin, W., Mao, C., Luan, X., Shen, D.D., Shen, Q., Su, H., Wang, X., Zhou, F., Zhao, W., Gao, M., et al. (2020). Structural basis for inhibition of the RNA-dependent RNA polymerase from SARS-CoV-2 by remdesivir. Science. 368(6498), 1499-1504. Published online 2020/05/03 DOI: 10.1126/science.abc1560.